Summer 2019

Efficient estimation and mitigation for radio-frequency interference

Qiaolei Huang

Department: Electrical and Computer Engineering

EFFICIENT ESTIMATION AND MITIGATION FOR RADIO-FREQUENCY INTERFERENCE

by

QIAOLEI HUANG

A DISSERTATION

Presented to the Faculty of the Graduate School of the

MISSOURI UNIVERSITY OF SCIENCE AND TECHNOLOGY

In Partial Fulfillment of the Requirements for the Degree

DOCTOR OF PHILOSOPHY

in

ELECTRICAL ENGINEERING

2019

Approved by:

Jun Fan, Advisor
Daryl Beetner
Chulsoon Hwang
Victor Khilkevich
Xiaoming He

PUBLICATION DISSERTATION OPTION

This dissertation consists of the following three articles, formatted in the style used by the Missouri University of Science and Technology:

Paper I: Pages 3-30 have been published on IEEE Transactions on Electromagnetic Compatibility.

Paper II: Pages 31-49 are intended for submission to IEEE Transactions on Electromagnetic Compatibility.

Paper III: Pages 50-77 have been published on IEEE Transactions on Electromagnetic Compatibility.

ABSTRACT

With rapid innovations in Internet of Things (IoT) and wireless technology, more and more consumer electronic devices around the world are now connected to the internet. In a small form factor electronic device, there are plenty of potential noise sources such as System On Chip (SoC), high speed traces, flexible cables and power converters, etc. Those noise sources can possibly introduce radio frequency interference (RFI) issues. In this dissertation, a transfer function based calculation method is proposed to estimate radio frequency interference (RFI) problems. The derived equations can clearly decompose the RFI problem into two parts: the noise source and the coupling transfer function to the antenna. The proposed method is validated through numeric simulations and real cellphone experiments. Based on this method, a novel RFI mitigation method is proposed. Through near-field scanning of a real product, an equivalent dipole moment of the noise source (CPU and DDR3) is reconstructed, and the near-field components of the victim (Wi-Fi antenna) are measured. By determining the relationship between dipole moment and antenna near field, the noise source is rotated by a certain angle to reduce RFI. New boards with the suggested changes are fabricated and the measured results show a good RFI reduction (up to 8 dB) compared to original boards. Novel machine learning method is also introduced to accurately extract equivalent dipole moments from the near field scanning of a noise source. Compared to the conventional least square method, the proposed machine learning based method is believed to have a better accuracy. Also, machine learning based method is more reliable in handling noise in practical applications.

ACKNOWLEDGMENTS

I would like to express my great gratitude to my advisor, Dr. Jun Fan, for his guidance, encouragement, and trust throughout my PhD studies. I learned a lot from him not only at the technical side, but also the non-technical side. He helped me gain a big picture of how to deal with research work, the people around, and also family. I feel fortunate to work with him and be his student.

I would like to thank Dr. Chulsoon Hwang. It was a great experience to work with him on many interesting RFI projects. I would also like to thank Dr. Beetner, Dr. Victor Khilkevich and Dr. Xiaoming He for their advice and help on my research work.

I also feel grateful to Yansheng Wang, Guangyao Shen, Xiang Fang, Liang Li, Xiangyang Jiao, Muqi Ouyang, Jiayi He and Jing Li. Every one of them helped me a lot in my research and life in Rolla. Also my thanks go to all of the other faculty members and my fellow lab mates in the EMC group of Missouri S&T. I am happy to work with you.

This dissertation is based upon work supported partially by the National Science Foundation under Grant No. IIP-1440110.

I am deeply grateful to my family. Thanks for their understanding and love all the time.

Finally, my sincere appreciation goes to my mother. I dedicate this dissertation to her.

TABLE OF CONTENTS

Page

LIST OF ILLUSTRATIONS

PAPER III

1. INTRODUCTION

With rapid innovations in Internet of Things (IoT) and wireless technology, more and more consumer electronic devices around the world are now connected to the internet. In a small form factor electronic device, there are plenty of potential noise sources such as System On Chip (SoC), high speed traces, flexible cables and power converters, etc. Those noise sources can possibly introduce radio frequency interference (RFI) issues. Predicting and mitigating RFI issues are important for design engineers. The first paper focuses on deriving an analytical method to predict RFI. The second paper uses the derived equations in the first paper and proposes methods to mitigate RFI. In the third paper, a novel machine learning method is introduced to build equivalent dipole moments to replace noise sources.

In the first paper, a transfer function based calculation method is proposed to estimate radio frequency interference (RFI) problems. The closed-form equations are analytically derived from Maxwell's equations and the reciprocity theorem. The derived equations can clearly decompose the RFI problem into two parts: the noise source and the coupling transfer function to the antenna. Engineering insights drawn from the method are also discussed. Overall, the proposed method is accurate, fast and can provide physical insights for practical designs.

In the second paper, a novel RFI mitigation method is proposed. Through near-field scanning, an equivalent dipole moment of the noise source (CPU and DDR3) is reconstructed, and the near-field components of the victim (Wi-Fi antenna) are measured. By determining relationship between dipole moment and antenna near field, the noise

source is rotated by a certain angle to reduce RFI. Rotating the source to reduce RFI is implemented in such a way that it doesn't compromise signal integrity, and it doesn't require an additional shield can. New boards with the suggested changes are fabricated and the measured results show a good RFI reduction (up to 8 dB) compared to original boards.

In the third paper, a new machine learning based source reconstruction method is developed to extract the equivalent dipole moments more accurately and reliably. Based on the near field patterns, the proposed method can determine the minimal number of dipole moments and their corresponding locations. Further the magnitude and phase for each dipole moment can be extracted. The proposed method can extract the dominant dipole moments for the unknown noise sources one by one. The proposed method is applied to a few theoretical examples first. The measurement validation using a test board and a practical cellphone are also given. Compared to the conventional LSQ method, the proposed machine learning based method is believed to have a better accuracy. Also, it's more reliable in handling noise in practical applications.

PAPER

I. A TRANSFER FUNCTION BASED CALCULATION METHOD FOR RADIO FREQUENCY INTERFERENCE

ABSTRACT

A transfer function based calculation method is proposed to estimate radio frequency interference (RFI) problems. The closed-form equations are analytically derived from Maxwell's equations and the reciprocity theorem. The derived equations can clearly decompose the RFI problem into two parts: the noise source and the coupling transfer function to the antenna. Based on derivations, a transfer function concept is proposed to quantify the coupling coefficient from each unit dipole moment to the victim antenna. The transfer functions can be easily obtained from S parameter measurements. The proposed method is validated through numeric simulations and real cellphone experiments. Engineering insights drawn from the method are also discussed. Overall, the proposed method is accurate, fast and can provide physical insights for practical designs.

1. INTRODUCTION

With rapid innovations in Internet of Things (IoT) and wireless technology, more and more consumer electronic devices around the world are now connected to the internet. In a small form factor electronic device, there are plenty of potential noise sources such as System On Chip (SoC), high speed traces, flexible cables and power

converters, etc. Those noise sources can possibly introduce radio frequency interference (RFI) issues. Generally, RF antennas often have a high sensitivity, so the allowable RFI levels (ranging from -90 dBm to -125 dBm for various wireless standards) are much lower than the allowable electromagnetic compatibility (EMC) emission levels specified in the FCC and other similar regulations [1]. The radio frequency interference often limits the usefulness of wireless devices, causing great inconvenience to users.

Lots of studies have been focused on understanding of particular interference problem in a developed system and developing effective numerical simulation methods [2]-[3]. As the analysis and diagnosis are based on their particular physical structures, it is widely believed that the RFI is an unpredictable area in a development stage where design decisions have to be made. As wireless devices become increasingly integrated and cost-sensitive, it is essential to develop a model to better explain the mechanism of RFI and provide a physical insight to development engineers.

RFI problems can be divided into two parts: the radiation sources and the coupling ratio to the victim antenna. Real noise sources, like ICs, are typically difficult to model due to its complexity. Recently, a lot of work has been done on the radiation source part to build equivalent noise source model. In [4], equivalent electric and magnetic currents are extracted to model the PCB emissions. In [5], a Huygens' equivalence method is used for RFI analysis. This method can be implemented in full wave simulation tools. However, theoretically, the Huygens's equivalence method requires the E or H field obtained on a closed surface. The measurement of near field E or H field scanning on a closed surface is often quite time-consuming and sometimes even impossible to achieve due to the geometry constraints of the electrical device. In addition, this method provides

little physical insight of the radiation source itself. This disadvantage is due to the property of the Huygens' equivalence theorem itself. It can only predict the EM field outside this Huygens' box and does not provide any information inside the box where the real noise exists.

An equivalent dipole moment model is applied in [6]-[10]. An array of electric and magnetic dipole moments is used to replace the radiation source. Usually near-field scanning measurement is performed to obtain one surface of E or H field above the noise source. Later an array of electric and magnetic dipole moments will be equivalently built to fit the measured near field data. In [6] and [7], a differential evolution optimization method is utilized. [8] applies a quantum particle swarm optimization (QPSO) algorithm to find dipole moments to equivalently model antennas. To increase the accuracy, [9] and [10] combines the traditional least square method with regularization and pattern recognition techniques to extract the dipole moments with physical meanings. In this way, the original coupling problem between the real noise source and the victim antenna can be equivalently regarded as the coupling between the dipole moment array and the victim antenna. The dipole moment array can be imported into full wave simulation tools [11]. By putting the equivalent dipole moment source model and the victim antenna model in a full wave simulation tool, its coupling relationship can be simulated. However, the simulation of a large number of dipole moment array takes a lot of time and computational resources [11]-[13].

In [14] and [15], the authors utilized the reciprocity method to decompose the RFI problem into two parts: the forward problem and the reverse problem. By measuring E and H field on a 6-surface box in the forward and reverse problem separately, the near

field coupling between the noise source and the victim antenna can be calculated. The method of [14] provides a hint to estimate RFI through this 2-step process. However, this 2-step E and H field measurements over a 6-surface box is time consuming and often not available in practical products. More importantly, this method can't separate the noise source and the transfer function.

In this paper, a transfer function based calculation method is proposed for fast and accurate RFI estimation. The proposed method can help understand both the noise source and the coupling transfer function to an antenna. The RFI problem is decomposed into two parts: the forward problem and reverse problem. Then, the RFI problem is analytically modeled by integrating the dipole moment source model into the reciprocity theorem. The proposed method can provide transfer functions for each equivalent dipole moment. Engineers can use equivalent dipole moments and corresponding transfer functions to answer several "what-if" questions and make design decisions. It can be also used for efficient numerical simulations. Regardless of the number of dipole moments, the coupling can be calculated very quickly and accurately. In case of experimental investigation, as only single surface near-field scanning is required, the measurement is much easier compared to 6-surface measurements in [14]. In addition, only S_{21} measurements are needed to obtain transfer functions.

This paper is organized as follows. In Section 2, a general RFI coupling model is formulated using the reciprocity theorem. Based on derivations, a transfer function concept to quantify the coupling coefficient from each unit dipole moment to the victim antenna is proposed. In addition, methods to obtain the transfer functions in simulations and measurements are addressed. In Section 3, the proposed method is validated through

numerical simulations. The method is further applied to estimate the noise coupling from an LCD panel to RF antennas in a practical cellphone. In Section 5 and 6, the engineering insights and conclusions are provided.

2. NEW RECIPROCITY METHOD FOR RFI ESTIMATION

In order to understand both the noise source and the coupling path to the victim antenna, the coupling problem is divided into two steps: the forward problem and the reverse problem, as shown in Figure 1. In the forward problem, the real noise source is turned on and the victim antenna is turned off. In the reverse problem, the antenna is excited and the noise source is turned off.

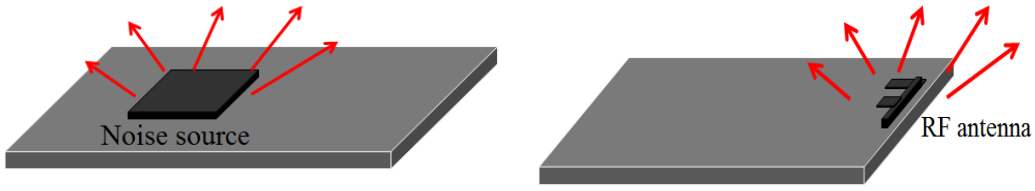

(a) (b)

Figure 1. A RFI problem is divided into two parts. (a) Forward problem: real noise source is radiating; antenna is terminated and turned OFF. (b) Reverse problem: victim antenna is turned on and radiate; real noise source is turned off

Assume in the forward problem, sources ($\vec{J}^{\,fwd}, \vec{M}^{\,fwd}$) produce fields ($\vec{E}^{\,fwd}, \vec{H}^{\,fwd}$). In reverse problem, sources ($\vec{J}^{\,rev}, \vec{M}^{\,rev}$) produce fields ($\vec{E}^{\,rev}, \vec{H}^{\,rev}$). According to [16], the most useful form of reciprocity theorem can be written as

$$\iiint_V \left(\vec{E}^{\,rev} \cdot \vec{J}^{\,fwd} - \vec{H}^{\,rev} \cdot \vec{M}^{\,fwd}\right) dv' = \iiint_V \left(\vec{E}^{\,fwd} \cdot \vec{J}^{\,rev} - \vec{H}^{\,fwd} \cdot \vec{M}^{\,rev}\right) dv' \qquad (1)$$

where V encloses an infinite large volume. In the forward problem, $\vec{J}^{fwd}, \vec{M}^{fwd}$ have non-zero values only in the noise source region. For the left side of equation (1), the volume integral over the entire region can be reduced to the volume integral over only the real noise source region V_s.

The source region is further divided into N small enough regions V_i. The volume integral of the electric current density $\vec{J}^{fwd}$ and magnetic current density $\vec{M}^{fwd}$ in a small enough region is essentially the definition of the electric and magnetic dipole moment. The left side of equation (1) can be derived as

$$\begin{aligned}
&\iiint_V \left(\vec{E}^{rev} \cdot \vec{J}^{fwd} - \vec{H}^{rev} \cdot \vec{M}^{fwd}\right) dv' \\
&= \iiint_{V_S} (\vec{E}^{rev} \cdot \vec{J}^{fwd} - \vec{H}^{rev} \cdot \vec{M}^{fwd}) dv' \\
&= \sum_{i=1}^{N} \iiint_{V_i} (\vec{E}^{rev} \cdot \vec{J}^{fwd} - \vec{H}^{rev} \cdot \vec{M}^{fwd}) dv' \\
&= \sum_{i=1}^{N} \left[\vec{E}_i^{rev} \cdot \iiint_{V_i} (\vec{J}^{fwd}) dv' - \vec{H}_i^{rev} \cdot \iiint_{V_i} (\vec{M}^{fwd}) dv' \right] \\
&= \sum_{i=1}^{N} (\vec{E}_i^{rev} \cdot \vec{P}_i^{fwd} - \vec{H}_i^{rev} \cdot \vec{M}_i^{fwd})
\end{aligned} \tag{2}$$

where $\vec{E}_i^{rev}$ is the E field at the i^{th} source region V_i. Since the electric dipole moment is defined for this small enough source region, $\vec{E}_i^{rev}$ can also be regarded as the E field at location of the i^{th} electric dipole moment.

Similarly, $\vec{H}_i^{rev}$ is the H field at the i^{th} source region and also the i^{th} magnetic dipole moment. $\vec{P}_i^{fwd}$ is the i^{th} electric dipole moment which has the unit of A·m. In the last line of (2), $\vec{M}_i^{fwd}$ is the i^{th} magnetic dipole moment which has the unit of V·m. The electric dipole moment and magnetic dipole moment are placed at discrete locations.

Same as [14], the first term of the right side of (1) can be derived as

$$\iiint_V (\vec{E}^{fwd} \cdot \vec{J}^{rev}) dv' = \iint_{S_a} (\vec{E}_a^{fwd} \cdot \vec{J}_a^{rev}) ds' = -I_a^{rev} \int_{r=D_1}^{r=D_2} \vec{E}_a^{fwd} \, dr = -I_a^{rev} U_a^{fwd} \tag{3}$$

In the reverse problem, $\vec{J}^{rev}$ and $\vec{M}^{rev}$ have non-zero values only at antenna's port surface S_a. The volume integral over the entire region can be reduced to the surface integral over the antenna's port surface S_a. $\vec{J}_a^{rev}$ is the electric surface current density on S_a. TEM mode is assumed at the antenna's port surface.

The line integral of $\vec{E}_a^{fwd}$ between the two conductors of the antenna port is voltage U_a^{fwd}. I_a^{rev} and U_a^{fwd} are the current and voltage at the antenna port in the reverse and forward problems, respectively. Similarly, the second term of the right side of (1) can be derived as

$$-\iiint_V (\vec{H}^{fwd} \cdot \vec{M}^{rev}) dv' = -\iint_{S_a} (\vec{H}_a^{fwd} \cdot \vec{M}_a^{rev}) ds' = -I_a^{fwd} \int_{r=D_1}^{r=D_2} \vec{E}_a^{rev} \, dr = -I_a^{fwd} U_a^{rev} \tag{4}$$

where the volume integral over the entire region can be reduced to the surface integral over the antenna's port surface S_a. $\vec{M}_a^{rev}$ is the magnetic surface current density on S_a. Equivalence theorem is applied on S_a to represent $\vec{M}_a^{rev}$ with $\vec{E}_a^{rev}$. I_a^{fwd} and U_a^{rev} are the current and voltage at the antenna port in the forward and reverse problems, respectively.

Assuming the antenna port is excited by a coaxial cable, the geometry is shown in Figure 2. R_1 and R_2 are the inner and outer radius of the coaxial cable. The detailed derivations for (3) and (4) for the coaxial port are shown in

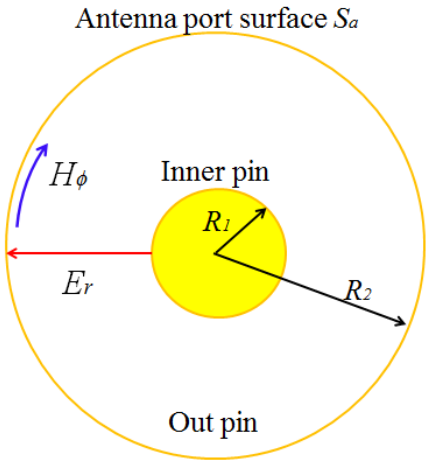

Figure 2. E and H fields on antenna port surface

$$
\begin{aligned}
&\iiint_V (\vec{E}^{\,fwd} \cdot \vec{J}^{\,rev}) dv' \\
&= \iint_{S_a} (\vec{E}_a^{\,fwd} \cdot \vec{J}_a^{\,rev}) ds' = \iint_{S_a} \vec{E}_a^{\,fwd} \cdot (\hat{n} \times \vec{H}_a^{\,rev}) ds' \\
&= \iint_{S_a} \hat{n} \cdot (\vec{H}_a^{\,rev} \times \vec{E}_a^{\,fwd}) ds' = \iint_{S_a} \hat{n} \cdot (H_\phi^{\,rev} \hat{\phi} \times E_r^{\,fwd} \hat{r}) ds' \\
&= \iint_{S_a} (-\hat{n} \cdot \hat{n}) H_\phi^{\,rev} \; E_r^{\,fwd} ds' = -\int_{r=R_1}^{r=R_2} H_\phi^{\,rev} E_r^{\,fwd} 2\pi r \; dr \\
&= -\int_{r=R_1}^{r=R_2} (H_\phi^{\,rev} 2\pi r) E_r^{\,fwd} \; dr = -I_a^{\,rev} U_a^{\,fwd}
\end{aligned}
\tag{5}
$$

$$
\begin{aligned}
&-\iiint_V (\vec{H}^{\,fwd} \cdot \vec{M}^{\,rev}) dv' \\
&= -\iint_{S_a} (\vec{H}_a^{\,fwd} \cdot \vec{M}_a^{\,rev}) ds' = -\iint_{S_a} \vec{H}_a^{\,fwd} \cdot (-\hat{n} \times \vec{E}_a^{\,rev}) \, ds' \\
&= \iint_{S_a} \hat{n} \cdot (\vec{E}_a^{\,rev} \times \vec{H}_a^{\,fwd}) ds' = \iint_{S_a} \hat{n} (\; E_r^{\,rev} \hat{r} \times H_\phi^{\,fwd} (-\hat{\phi})) ds' \\
&= -\iint_{S_a} \hat{n} \cdot (\hat{n}) E_r^{\,rev} \; H_\phi^{\,fwd} ds' = -\int_{r=R_1}^{r=R_2} H_\phi^{\,fwd} E_r^{\,rev} 2\pi r \; dr \\
&= -\int_{r=R_1}^{r=R_2} (H_\phi^{\,fwd} 2\pi r) E_r^{\,rev} \; dr = -I_a^{\,fwd} U_a^{\,rev}
\end{aligned}
\tag{6}
$$

Combining (3) and (4), the right side of (1) becomes

$$\begin{aligned}
&\iiint_V \left(\vec{E}^{\,fwd}\cdot\vec{J}^{\,rev}-\vec{H}^{\,fwd}\cdot\vec{M}^{\,rev}\right)dv' \\
&=-I_a^{rev}U_a^{fwd}-I_a^{fwd}U_a^{rev}=-\frac{U_a^{rev}}{Z_{in}}U_a^{fwd}-\frac{U_a^{fwd}}{Z_L}U_a^{rev} \\
&=-\frac{Z_L+Z_{in}}{Z_{in}Z_L}U_a^{fwd}U_a^{rev}=-U_a^{fwd}\frac{Z_L+Z_{in}}{Z_{in}Z_L}(1+\Gamma)U_a^{rev(+)} \\
&=-U_a^{fwd}\frac{Z_L+Z_{in}}{Z_{in}Z_L}\left(\frac{2Z_{in}}{Z_{in}+Z_0}\right)U_a^{rev(+)}=-\frac{2}{Z_L}U_a^{fwd}U_a^{rev(+)}
\end{aligned} \tag{7}$$

where Z_{in} is the input impedance of the RF antenna in the transmitting mode in the reverse problem. Z_L is the receiver impedance at the antenna port in the receiving mode in the forward problem, which is typically 50Ω. U_a^{rev} uses the total voltage definition. It can be replaced with the incident voltage wave $U_a^{rev(+)}$ and reflection coefficient Γ. Z_0 is the characteristic impedance of the coaxial cable, which is typically 50 Ω.

Substituting (2) and (7) back into (1) results in

$$\sum_{i=1}^{N}\left(\vec{E}_i^{\,rev}\cdot\vec{P}_i^{\,fwd}-\vec{H}_i^{\,rev}\cdot\vec{M}_i^{\,fwd}\right)=-U_a^{fwd}U_a^{rev(+)}\frac{2}{Z_L} \tag{8}$$

The coupled voltage U_a^{fwd} induced at the RF antenna port due to the noise source, can be written as

$$U_a^{fwd}=\sum_{i=1}^{N}\left(-\vec{E}_i^{\,rev}\frac{Z_L}{2U_a^{rev(+)}}\right)\cdot\vec{P}_i^{\,fwd}+\sum_{i=1}^{N}\left(\vec{H}_i^{\,rev}\frac{Z_L}{2U_a^{rev(+)}}\right)\cdot\vec{M}_i^{\,fwd} \tag{9}$$

where $U_a^{rev(+)}$ is the incident voltage in the reverse problem. In the reverse problem, when antenna is excited by a incident voltage wave of $U_a^{rev(+)}$, $\vec{E}_i^{\,rev}$ is measured at location of

the i^{th} electric dipole moment and $\vec{H}^{rev}$ is measured at the location of the i^{th} magnetic dipole moment. Z_L is 50Ω. It is worth noting that a linear relationship can be established between each dipole moment and the final coupled voltage. A transfer function concept is then introduced here to quantify the coupling relationship from each dipole moment to the victim antenna.

$$U_a^{fwd} = \sum_{i=1}^{N} \vec{f}_{P_i} \cdot \vec{P}_i^{fwd} + \sum_{i=1}^{N} \vec{f}_{M_i} \cdot \vec{M}_i^{fwd} \tag{10}$$

where $\vec{f}_{P_i}$ is for each electric dipole moment $\vec{P}_i^{fwd}$ and $\vec{f}_{M_i}$ is for each magnetic dipole moment $\vec{M}_i^{fwd}$. $\vec{f}_{P_i}$ has a linear relationship with $\vec{E}_i^{rev}$, and $\vec{f}_{M_i}$ has a linear relationship with $\vec{H}_i^{rev}$, as shown in

$$\vec{f}_{P_i} = -\frac{Z_L}{2U_a^{rev(+)}} \vec{E}_i^{rev},\ \vec{f}_{M_i} = \frac{Z_L}{2U_a^{rev(+)}} \vec{H}_i^{rev} \tag{11}$$

From (11), the transfer functions $\vec{f}_{P_i}$ and $\vec{f}_{M_i}$ can be obtained as long as E and H field are acquired in the reverse problem. In a full wave simulation, acquiring E and H field in the reverse problem is straightforward by exciting the victim antenna. Once E and H field is obtained and plugged back in the equation, transfer functions are obtained.

The transfer functions are also relatively easy to obtain in measurements. The E and H fields measured by a near field probe at the each electric and magnetic dipole moment location can be expressed as

$$E_{x(i)}^{rev} = PF_E \cdot V_{E_x(i)},\ \ H_{x(i)}^{rev} = PF_H \cdot V_{H_x(i)} \tag{12}$$

where $E_{x(i)}^{rev}$ are x components of $\vec{E}_i^{rev}$. Also, $H_{x(i)}^{rev}$ are x components of $\vec{H}_i^{rev}$. PF_E and PF_F are the probe factor of E field probe and H field probe, respectively. $V_{E_x(i)}$ is the measured voltage on the instrument when measuring E_x at the location of i^{th} electric dipole moment in the reverse problem. $V_{H_x(i)}$ is the measured voltage on the instrument when measuring H_x the location of i^{th} magnetic dipole moment in the reverse problem. Substituting (12) into (11), transfer functions can be expressed in terms of several measureable terms

$$f_{P_x(i)} = -\frac{Z_L \cdot PF_E}{2} S_{21E_x(i)}^{rev},\ f_{M_x(i)} = \frac{Z_L \cdot PF_H}{2} S_{21H_x(i)}^{rev} \tag{13}$$

where $S_{21E_x(i)}^{rev}$ and $S_{21H_x(i)}^{rev}$ are the VNA measurements for E_x and H_x at the location of i^{th} dipole moment in the reverse problem, respectively. For the y and z components, similar relationships can be established. In the reverse problem, port one of VNA is connected to the victim antenna for the excitation, port two is connected to the E or H field probes. Since Z_L and the probe factors are constant values, the transfer functions are proportional to the corresponding S_{21} measurements.

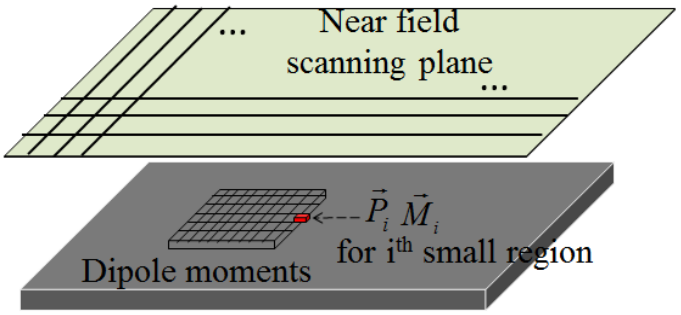

Figure 3. Equivalent dipole moment extraction using near field scanning

Once the transfer functions are obtained in the reverse problem, the coupling relationships between each unit dipole moment to the victim antenna can be obtained. In order to calculate coupling to the antenna, the forward problem is needed to obtain the equivalent dipole moment model for the real noise source. These are $\vec{P}_i^{fwd}$ and $\vec{M}_i^{fwd}$ in (10). $\vec{P}_i^{fwd}$ and $\vec{M}_i^{fwd}$ can be obtained by source reconstruction using the scanned near fields. The near field scanning is performed above the real noise source in the forward problem. An array of electric and magnetic dipole moments $\vec{P}_i^{fwd}$ and $\vec{M}_i^{fwd}$ can then be equivalently chosen to fit the measured near field data, as shown in Figure 3. Least square method will be utilized to reconstruct equivalent dipole moments because of its advantages of fast calculation time and effectiveness. In Figure 3, the noise source is divided into N small enough region, there is an electric dipole moment and a magnetic dipole moment assigned to each small region. The following linear relationship between the measured H-field and the dipole moment sources can be established

$$\begin{bmatrix} [H_x]_{K\times 1} \\ [H_y]_{K\times 1} \end{bmatrix} = [T]_{2K\times 6N} \begin{bmatrix} [P_x]_{N\times 1} \\ [P_y]_{N\times 1} \\ [P_z]_{N\times 1} \\ [M_x]_{N\times 1} \\ [M_y]_{N\times 1} \\ [M_z]_{N\times 1} \end{bmatrix} \tag{14}$$

where K is the number of the measured points on the near field scanning plane. N is also the number for each type of dipole moment. H_x and H_y are measured H fields at those K scanning points. Each element in the T matrix denotes the contribution of one type of the

dipole moment to one component of the magnetic field. *T* can be easily obtained once the locations of the observations plane and the dipole moment source are known [10]. (14) can also be simplified as

$$F = T \times X \tag{15}$$

where *F* is the measured H fields with the size of *2K×1*. T is the transfer function with the size of *2K×6N*. Moreover, *X* is the unknowns for all of the electric and magnetic dipole moments with the size of *6N×1*. The least square method is applied here to solve the inverse problem. The solution is

$$X = (T^t T)^{-1} T^t F \tag{16}$$

Once the equivalent dipole moments are obtained in the forward problem and transfer functions are obtained in the reverse problem, coupled voltage on the antenna port can be calculated using (10). It's worthwhile to mention that other dipole moment extraction methods in [6]-[10] are also valid as long as the extracted dipole moments have physical meanings and can reproduce the similar near fields.

3. NUMERICAL SIMULATION

From A two-layer PCB is built in a full wave simulation tool to verify the proposed method. The victim antenna is a patch antenna. The radiation sources contain two ideal dipole moments: a magnetic dipole moment and an electric dipole moment which are placed at different locations. The magnetic dipole moment is an infinitely small current loop facing x-direction with the magnitude of 1 V·m. The electric dipole moment is an infinitely small current segment facing z-direction with the magnitude of 0.001 A·m. Two

dipole moments are in phase. The detailed geometry is shown in Figure 4. According to (10), in order to calculate coupled voltage from the noise source to the victim antenna, dipole moments from the forward problem are needed. Also, transfer functions based on E and H field of the reverse problem are needed. In this simulation model, (10) can be simplified to

$$U_a^{fwd} = \vec{f}_P \cdot \vec{P} + \vec{f}_M \cdot \vec{M} = \frac{-Z_L}{2U_a^{rev(+)}} E_z^{rev} P_z + \frac{Z_L}{2U_a^{rev(+)}} H_x^{rev} M_x \tag{17}$$

P_z and M_x are 0.001 A·m and 1 V·m in this example. In the reverse problem, the ratio of H_x^{rev} to $U_a^{rev(+)}$ always stays the same with different $U_a^{rev(+)}$ excitations.. This is reasonable as the ratio of H_x^{rev} to $U_a^{rev(+)}$ represent the property of the antenna, which is always the same no matter what excitation the antenna has. The ratio of E_z^{rev} to $U_a^{rev(+)}$ has the same property. The predicted coupling voltage using (17) is compared with direct simulation results. The comparison is shown in Figure 5. The maximum error in this simulation example is 0.3 dB, which shows the validity of the proposed method.

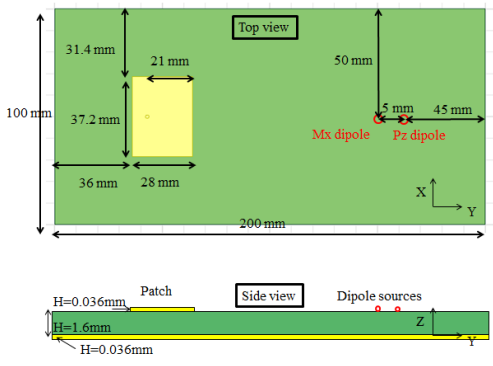

Figure 4. Geometry information for the simulation model

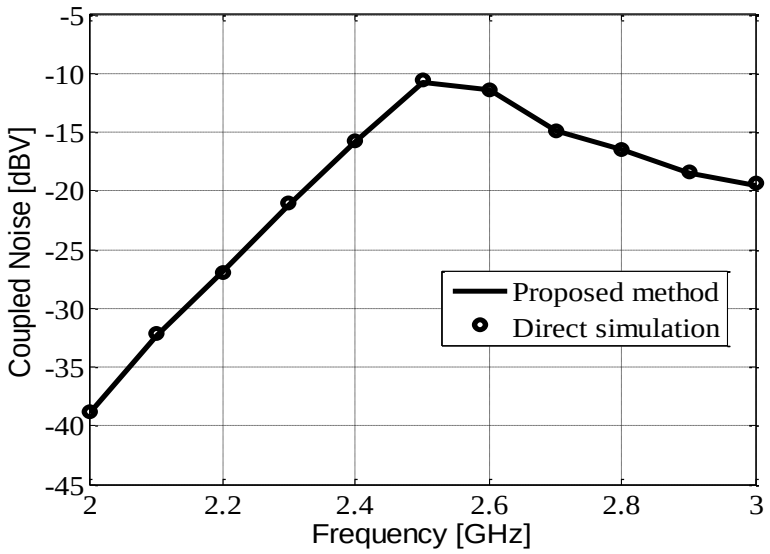

Figure 5. Coupled noise comparison between direct simulation and proposed method

4. PRACTICAL CELLPHONE CASE

The proposed method is applied to estimate the noise coupling from an LCD panel to an RF antenna in a practical cellphone, as used in [17]. The cellphone under test mainly consists of three parts: an LCD, a main body and a flex printed circuit board (FPCB), as shown in Figure 6. There are two antennas on the cellphone: the main antenna and the sub antenna. The high speed mobile industry processor interface (MIPI) display serial interface (DSI) signals routed on the FPCB are the noise source and couple to the two antennas. At the edge of the FPCB, a discontinuity of the ground plane is observed, as shown in Figure 7. According to [17], the noise source in this RFI problem can be equivalently modelled as a single M_y dipole moment. In a few other projects as shown in Figure 8, one single magnetic dipole moment is used to replace the noise source

according to its H field patterns. It's worthwhile to mention that the RFI measurement condition is this paper is almost the same as in a compact cellphone in the working condition, where the display and FPCB is placed on top of the main body. On the contrary, [17] uses a simplified measurement setup where display and FPCB are placed outside of the cellphone.

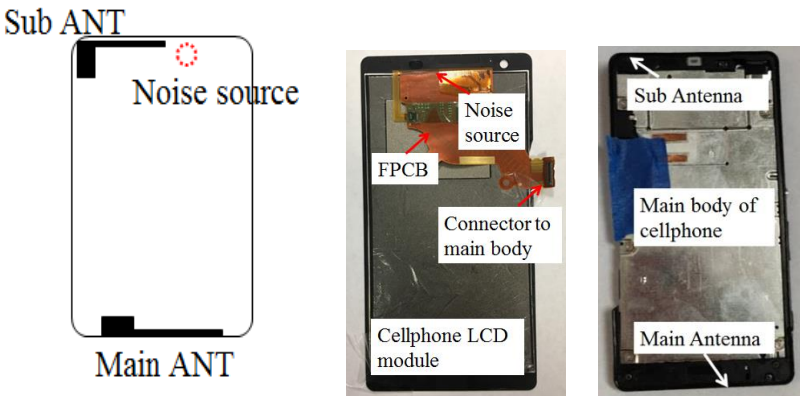

Figure 6. Illustration of the DUT

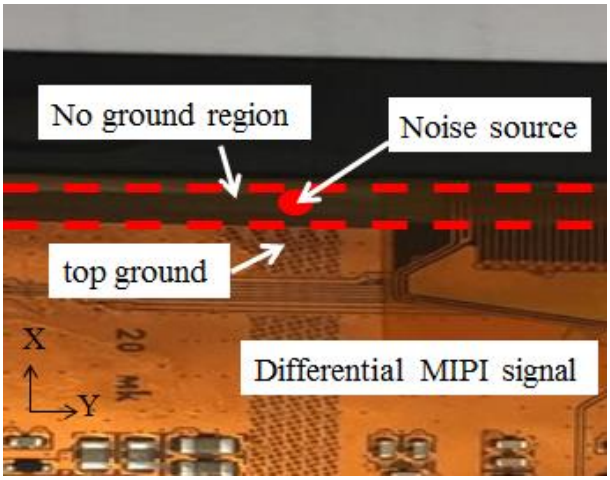

Figure 7. Magnetic dipole moment M_y caused by ground discontinuity in FPCB

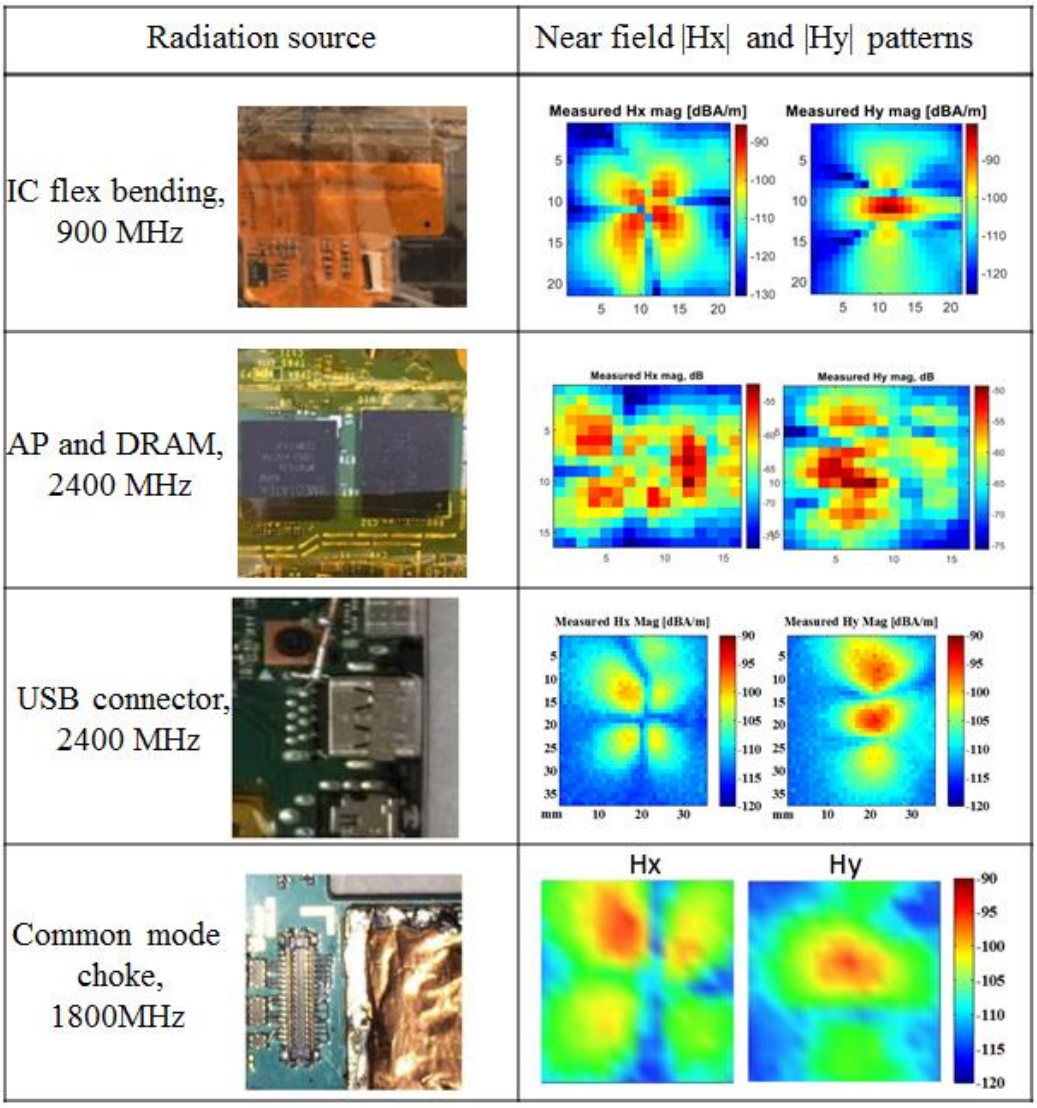

Figure 8. A single magnetic dipole moment to represent the noise source in different projects

A 3-step process was performed to validate the proposed method in this cellphone measurement, as shown in Figure 9. The coupled noise from the LCD panel to the antennas will be estimated using the proposed method and later compared with direct measurement results.

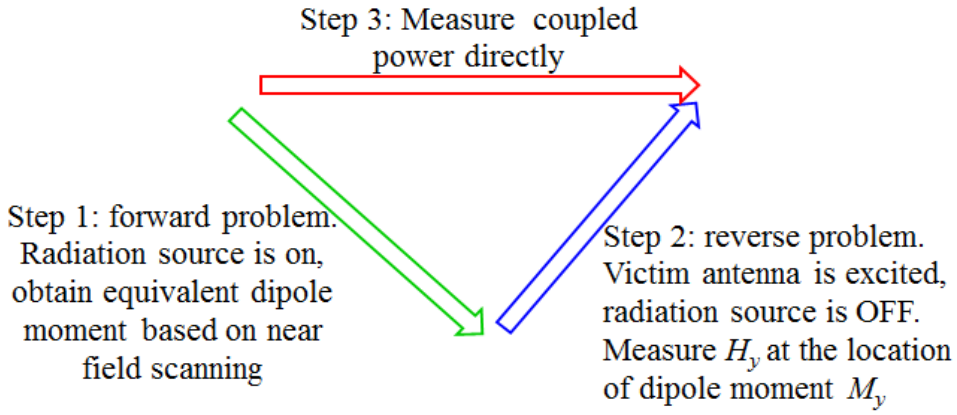

Figure 9. Workflow to validate the proposed method by measuring the cellphone

In step one, LCD was put into working condition. Radiation source was on. To obtain the phase-resolved H field data in the near field, the tuned receiver mode of the VNA was used [11]. In the tuned receiver mode, both of the two ports of the VNA worked as receivers. Two H field probes were connected to the each port of the VNA. The scanning plane was 40 mm × 40 mm with a scanning step of 2 mm. The scanning height was 2 mm above the FPCB. The measurement setup is shown in Figure 10.

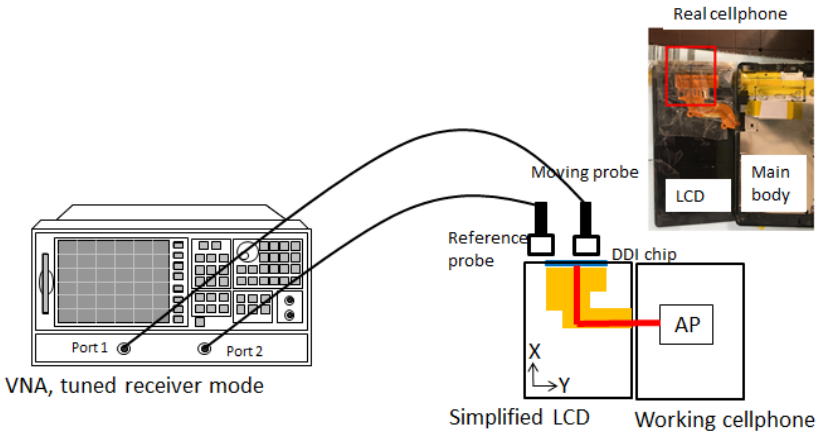

Figure 10. Phase-resolved near field scanning setup for the forward problem

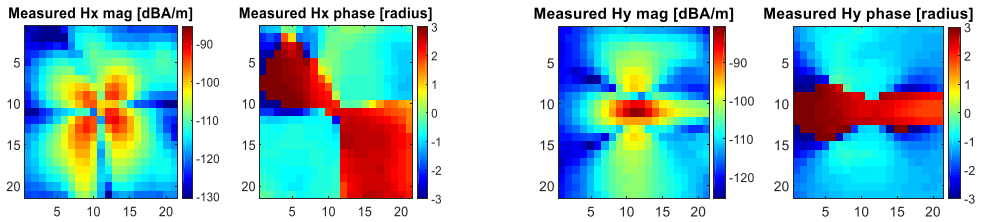

(a)

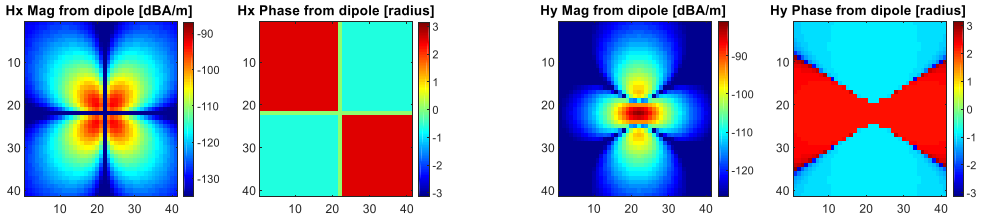

(b)

Figure 11. Magnitude and phase of H field in forward problem: (a) Measurement, (b) Reconstructed dipole moment M_y

The measured phase-resolved H field data were used to reconstruct the magnetic dipole moment M_y using the least square method in (16) by locating the single dipole moment M_y at the broken ground location. The H fields from measurement and the reconstructed dipole moment M_y are shown in Figure 11. A reasonably good agreement between the measured H field and the reconstructed dipole-generated H field supports that the reconstructed dipole can represent the real noise source. It's worthwhile to mention that the extracted dipole moment has both magnitude and phase in this example. However, as there is only one single dipole moment, the phase is not important when calculating the coupled power to the antenna.

In step two, the victim antenna radiates in the reverse problem. Because only magnetic dipole M_y exists in this problem, only y-component of H field is needed to estimate coupled voltage according to the inner product in (10). In this problem, (10) can be simplified to

$$U_a^{fwd} = \vec{f}_M \cdot \vec{M} = \frac{Z_L}{2U_a^{rev(+)}} H_y^{rev} M_y \tag{18}$$

where H_y^{rev} can be measured using a near field H probe. (18) can be expressed by several measureable terms:

$$U_a^{fwd} = \frac{Z_L PF_H}{2} S_{21H_y}^{rev} M_y \tag{19}$$

where PF_H is the probe factor of H field probe. $S_{21H_y}^{rev}$ is the measured S-parameter on VNA when measuring H_y in the reverse problem. The H_y location is the location of the dipole moment M_y obtained in the forward problem. In the reverse problem, port one is connected to the victim antenna for excitation, port two is connected to the H field probe. By performing a S_{21} measurement, the transfer function from the unit magnetic dipole M_y to the victim antenna can be obtained. The setup for the reverse problem is shown in Figure 12. Theoretically, H_y^{rev} should be measured at the exact location of the equivalent dipole moment M_y which is often inside an IC. In reality, the H field probe often cannot be put inside an IC due to the physical constraints. Here the H field probe is placed as close to the location of the dipole moment as possible. In order to test robustness of measurement setup, the H field probe was moved up several mm to test the variation of measured H field; the results were within 1 dB.

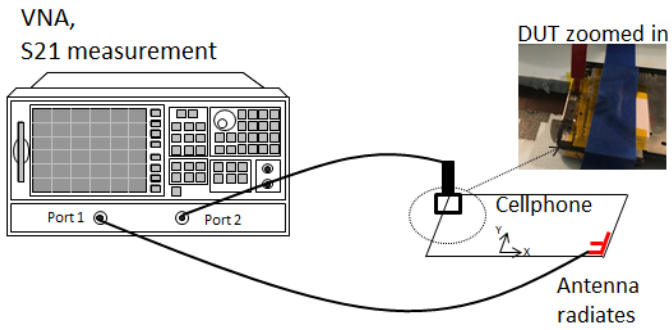

Figure 12. Measurement setup for the reverse problem

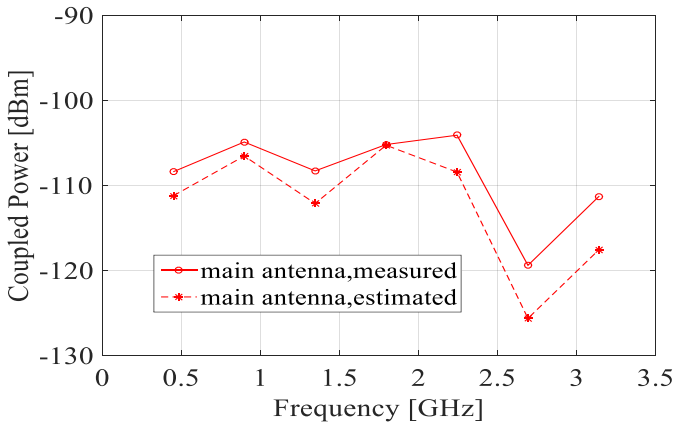

(a)

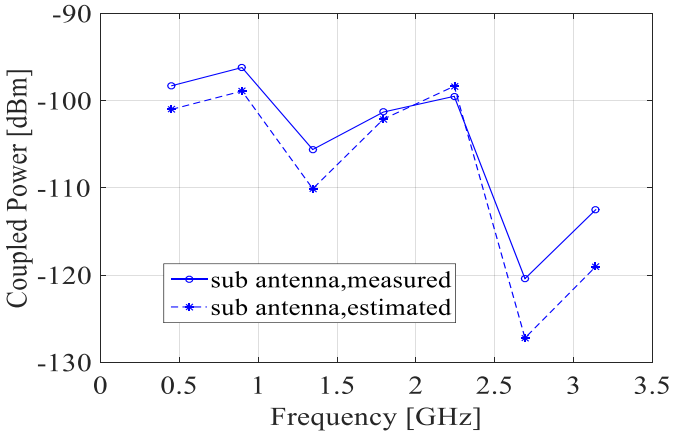

(b)

Figure 13. Measured and estimated coupled power to the antennas: (a) main antenna, (b) sub antenna

After finishing step one and two, M_y in the forward problem and H_y in the reverse problem can be obtained. Using (18), coupled voltage on the antenna port can be calculated. In step three, direct measurement of the coupled power is performed to compare with the estimated coupled value. As the noise source is from the clock harmonics of 448.5 MHz, the whole process is repeated for the first seven harmonics of the fundamental frequency. Estimated results are compared with measurement results, as shown in Figure 13 (a).

Besides the main antenna, there exists another sub antenna in this cellphone. Same procedures were performed to estimate the coupled power through the forward problem and the reverse problem. The estimated coupled power from the proposed method is compared with measurements in Figure 13(b).

For both of the two antennas, estimation errors are mostly within 6 dB. The relatively large error, especially at 3.115GHz is probably caused by the relatively low signal noise ratio in the forward problem where measurement accuracy of the weak near field is not good enough.

Also, in the reverse problem, the H field can't be measured at the exact location of the dipole moment due to the geometry constraint of the cellphone. In addition, the electrical size of the radiation geometry becomes larger at higher frequency; it might introduce additional errors if only one single dipole moment is used as equivalent source.

However, the overall estimation accuracy and the trend agreement are acceptable. The proposed method is successfully validated through the measurements using a practical cellphone.

5. DISCUSSION

In practice, engineers often need to know how much improvement a certain design change would make. The proposed method can help engineers answer those questions and make accurate and fast decisions. As mentioned, RFI problems contain two parts: the noise source and the coupling transfer function to the victim antenna. In our study here, the question of the coupling to the antenna is rigorously addressed. The transfer function concept can quantify the coupling from each unit dipole moment to the antenna. It also turns out that the transfer function is relatively easy to obtain from a simple S_{21} measurement.

One example is to find the best placement of the radiation source to minimize the RFI. For example, a cellphone and its antenna model is shown in Figure 14. Figure 14(b) and (c) show the magnitude of H_y and H_x at 1 GHz when the antenna radiates. If the noise source is identified as a M_y dipole moment, according to (18), the transfer function from each unit M_y dipole moment to the victim antenna is proportional to H_y in the reverse problem. So among the given locations 1, 2 and 3, location 1 has the smallest transfer function and location 3 has the largest transfer function. On the RFI perspective, location 1 will be the best place to locate the noise source M_y dipole moment where the coupling between M_y dipole moment to the victim antenna is the smallest.

The proposed method can also help understand rotation effect of the noise source. For example, suppose that noise source is fixed at location 2. By rotating the noise source 90°, M_y dipole moment becomes M_x dipole moment.

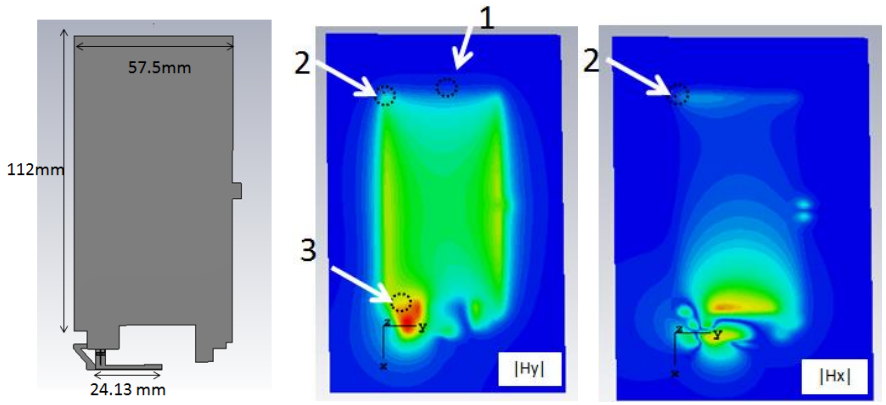

(a) (b) (c)

Figure 14. (a) A typical cellphone antenna model, (b) magnitude of H_y when the antenna radiates (c) magnitude of H_x when the antenna radiates

According to (18), the transfer function from each unit M_x dipole moment to the victim antenna is proportional to H_x in the reverse problem. Figure 14(c) shows the magnitude of H_x when the antenna radiates. Since H_x is much weaker than H_y at location 2, the transfer function is much weaker after rotating the noise source by 90˚. So for this particular antenna at 1 GHz, rotating the original noise source M_y by 90˚ will help reduce RFI a lot.

The rotation effect of an arbitrary angle is also of interest. For the simulation example in Figure 4, if the noise source only has one ideal magnetic dipole moment M_y. By rotating this current loop to different angles, the coupling to the victim antenna is different. It's worthwhile to investigate the best rotation angle to achieve the smallest RFI. The rotation of the magnetic dipole moment corresponds to different routing angles of the noise traces, or different angle placement of noise IC in real world applications. If the magnetic dipole is rotating to a certain angle in the xy-plane while the magnitude

keeps the same, the magnetic dipole moment will have both x- and y- components. Then calculated RFI can be written as

$$U_a^{fwd} = \frac{Z_L}{2U_a^{rev(+)}} \vec{H}_{\tan}^{rev} \vec{M}_{\tan}^{fwd} = \frac{Z_L}{2U_a^{rev(+)}} |\vec{H}_{\tan}^{rev}||\vec{M}_{\tan}^{fwd}| \hat{a}_{M_{\tan}} \cdot \hat{a}_{H_{\tan}} \quad (20)$$

where $|\vec{H}_{\tan}^{rev}|$ is the magnitude of tangential H field in the reverse problem when antenna is excited by an incident voltage of $U_a^{rev(+)}$. $|\vec{M}_{\tan}^{fwd}|$ is the magnitude of magnetic dipole moment in the forward problem. $\hat{a}_{M_{\tan}}$ and $\hat{a}_{H_{\tan}}$ are the unit vector along $\vec{H}_{\tan}^{rev}$ and $\vec{M}_{\tan}^{fwd}$, respectively.

For all the rotation angles, the scalar terms in (20) remain the same. The only changing term in (20) is the dot product of two unit vectors. It's worthwhile to mention that $\hat{a}_{M_{\tan}}$ and $\hat{a}_{H_{\tan}}$ have complex number terms. With different rotation angles of the magnetic dipole moment source, the coupled voltage calculated from (20) is compared with full wave simulation results, as shown in Figure 15. A good agreement between proposed method and the direct simulation result is observed. The error between our method and the direct simulation is within 0.3 dB. This further demonstrates the correctness of the proposed method.

The optimal angle finding method can also be utilized in real world applications. For example in the cellphone example in Figure 14, designers can utilize both the movement and rotation of noise source to minimize RFI. In addition, the antenna can also be slightly moved to obtain a minimal RFI while keeping the far field antenna parameters the same.

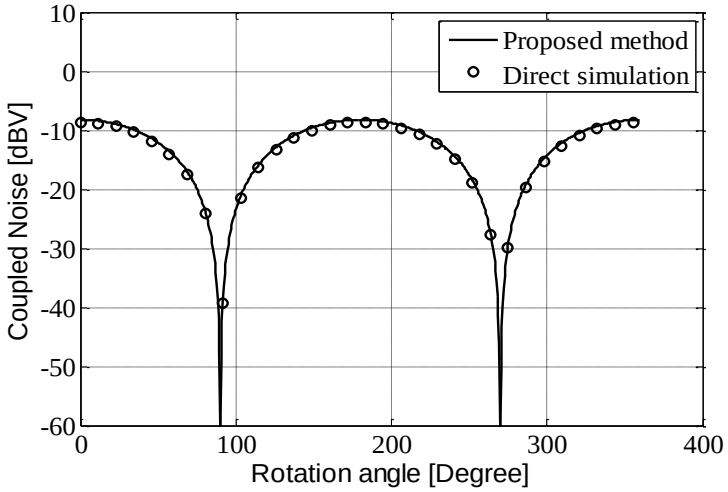

Figure 15. Coupled noise change due to the rotation effect of a magnetic dipole moment source

6. CONCLUSION

In this paper, a transfer function based calculation method is proposed to estimate RFI problems. The closed-form equations are analytically derived from Maxwell's equations and the reciprocity theorem. The RFI problem is decomposed into two parts: the noise source dipole moments and the coupling transfer function to the antenna. The transfer functions can be easily obtained from either simulation or measurement. Simple S_{21} measurements can help obtain transfer functions. The proposed method is validated through numeric simulations and real cellphone experiments. Engineers can utilize this method to identify root causes and propose mitigation solutions for RFI issues.

REFERENCES

[1] J. Fan, "A new EMC challenge: Intra-system RMI and RF interference," in *Safety and EMC*, pp. 1-3, 2015.

[2] H. H. Park, "Reduction of Electromagnetic Noise Coupling to Antennas in Metal-Framed Smartphones Using Ferrite Sheets and Multi-Via EBG Structures," *IEEE Trans. Electromagn. Compat*., vol. 60, no. 2, pp. 394-401, Apr. 2018.

[3] S.Shinde *et al*., "Investigation of interference in a mobile phone from a DC-to-DC converter," in *Proc. of IEEE Int. Symp. Electromagn.Compat*., 2013, pp. 616-620.

[4] P. Li and L. J. Jiang, "Source Reconstruction Method-Based Radiated Emission Characterization for PCBs," *IEEE Trans. Electromagn. Compat*., vol. 55, no. 5, pp. 933-940, Oct. 2013.

[5] L. Li et al., "Near-field coupling estimation by source reconstruction and Huygens's equivalence principle," in Proc. of IEEE Int. Symp. Electromagn.Compat., 2015, pp. 324-329.

[6] S. Gao, B. Wang, H. Zhao, W. Zhao, and C.E. Png, “Installed radiation pattern of patch antennas: Prediction based on a novel equivalent model,” IEEE Antennas Propag. Mag., vol. 57, pp. 81–94, June 2015.

[7] W. Zhao, E. Liu, B. Wang, S. Gao and C. E. Png, "Differential Evolutionary Optimization of an Equivalent Dipole Model for Electromagnetic Emission Analysis," *IEEE Trans. Electromagn. Compat*., vol. 60, no. 6, pp. 1635-1639, Dec. 2018.

[8] K. S. M. Mikki and A. A. Kishk, “Theory and applications of infinitesimal dipole models for computational electromagnetics,” IEEE Trans. Antennas Propag., vol. 55, no. 5, pp. 1325–1337, 2007.

[9] Q. Huang and J. Fan, "Machine Learning Based Source Reconstruction for RF Desense,"*IEEE Trans. Electromagn. Compat*., vol. 60, no. 6, pp. 1640-1647, Dec. 2018.

[10] Z. Yu, J. A. Mix, S. Sajuyigbe, K. P. Slattery and J. Fan, “An improved dipole-moment model based on near-field scanning for characterizing near-field coupling and far-field radiation from an IC,” *IEEE Trans. Electromagn. Compat*., vol. 55, no. 1, pp. 97-108, Feb. 2013.

[11] Q. Huang, *et al*., “Radio frequency interference estimation using transfer function based dipole moment model," in *Proc. of IEEE Asis-Pac. Symp. Electromagn.Compat*., 2018, pp. 115-120.

[12] C. Wu *et al*., "Estimating the near field coupling from SMPS circuits to a nearby antenna using dipole moments," in *Proc. of IEEE Int. Symp. Electromagn.Compat*., 2016, pp. 353-357.

[13] J. Pan *et al*., "Application of dipole-moment model in EMI estimation," in *Proc. of IEEE Int. Symp. Electromagn.Compat*., 2015, pp. 350-354.

[14] H. Wang, V. Khilkevich, Y. Zhang and J. Fan, "Estimating radio-frequency interference to an antenna due to near-field Coupling using decomposition method based on reciprocity," *IEEE Trans. Electromagn. Compat*., vol. 55, no. 6, pp. 1125-1131, Dec. 2013.

[15] S. Lee, *et al*., "Analytical intra-system EMI model using dipole moments and reciprocity," in *Proc. of IEEE Asis-Pac. Symp. Electromagn.Compat*., 2018, pp. 1169-1173.

[16] A. B. Constantine, *Advanced Engineering Electromagnetics*. New York, NY, USA: Wiley, 2012.

[17] Q. Huang, F. Zhang, T. Enomoto, J. Maeshima, K. Araki and C. Hwang, "Physics-based dipole moment source reconstruction for RFI on a practical cellphone", *IEEE Trans. Electromagn. Compat*., vol. 59, no. 6, pp. 1693-1700, Dec. 2017.

II. EFFICIENT RFI MITIGATION USING ROTATION FOR DDR NOISE SOURCE

ABSTRACT

In modern wireless consumer electronic devices, there is an increasing need for smaller, compact, and denser design. This often requires wireless components like transceiver, front-end and antenna to be placed very close to noise sources like memory, power supply, and main processor in the device. Electromagnetic noise from noise sources interferes with wireless receiver components causing radio frequency interference (RFI) issues in the device. As a result, wireless performance metrics like range and throughput is degraded, which impacts the user experience. In this paper, a popular consumer electronic device is studied. The device has many complex subsystems like CPU, DDR memory, and power supply co-located with Wi-Fi circuitry. Due to small size, the device has RFI issues from CPU memory interface, which affects the Wi-Fi range. Typically, RFI problem can be mitigated from a mechanical design perspective by adding shield can, or from a signal integrity perspective by modifying clock and slew rate of the high-speed signals. In this paper, a novel RFI mitigation method is proposed. Through near-field scanning, an equivalent dipole moment of the noise source (CPU and DDR3) is reconstructed, and the near-field components of the victim (Wi-Fi antenna) are measured. By determining relationship between dipole moment and antenna near field, the noise source is rotated by a certain angle to reduce RFI. Rotating the source to reduce RFI is implemented in such a way that it doesn't compromise signal integrity, and it doesn't require an additional shield can. New boards with the suggested changes are

fabricated and the measured results show a good RFI reduction (up to 8 dB) compared to original boards.

1. INTRODUCTION

With the recent progress in Internet of Things (IoT), several consumer electronic devices around the world are now connected to the Internet. These devices range from a refrigerator to a small car key fob, which is connected wirelessly to the internet access point through Wi-Fi. Although wireless technology in IoT devices provides great convenience, it also brings a lot of design challenges to RF integration engineers. As the complexity of digital subsystem increases, potential noise sources in devices such as microcontroller unit (MCU), System On Chip (SoC), high-speed traces, flexible cables, and power converters couples to a co-located wireless antenna. This unintended electromagnetic noise, called RF interference (or simply RFI) interferes the functionality of wireless radio and reduces the usable wireless range of the device.

There are a few conventional ways to mitigate RFI. For example, designers use shield can and grounding schemes to suppress noise radiation by modifying the coupling path. However, in small form-factor products, it is difficult to use a shield can due to mechanical (product design) fabrication and cost limitations.

Another approach is to modify the noise source itself. Clock or slew rate can be lowered to reduce the power spectral density (PSD) of noise source in the frequency where RFI issues occur. However, modifying signal quality may reduce the signal integrity margin. A third approach is to route high-speed signals in a stripline fashion,

instead of a microstrip. A stripline structure can provide better shielding compared to a microstrip structure.

However, the choice of using a stripline routing or a microstrip routing can increase the PCB layer count, affect signal integrity, and also add complexity to the overall board layout. Therefore, it is important to explore alternate ways to mitigate RFI without compromising signal integrity or adding cost to the product.

Recently, efficient methods to predict RFI in a real product have been introduced in [1] and [2]. Reciprocity theorem is used to estimate RFI by decomposing the overall problem into two steps - forward problem and reverse problem.

In the forward problem, the noise source's near-field radiation is studied while the victim antenna is terminated. The forward problem can reconstruct noise source into an equivalent dipole moment model. In the reverse problem, the antenna is excited and the noise source is turned off. Using the equivalent dipole moment and the reverse field, RFI from noise source to antenna can be obtained. However, there has been little effort to conduct a systematic way to mitigate RFI.

In this paper, a popular consumer electronic device is studied. This small form-factor device has many complex digital sub-systems, including CPU, DDR memory, power supply, and two Wi-Fi antennas (for MIMO functionality) as shown in Figure 1. Through measurements, it is determined that high speed DDR3 traces on the main logic board is the dominant noise source for RFI issue on the Wi-Fi antennas. Having identified the noise, the below outlined steps are followed to measure, reconstruct, and mitigate RFI issue.

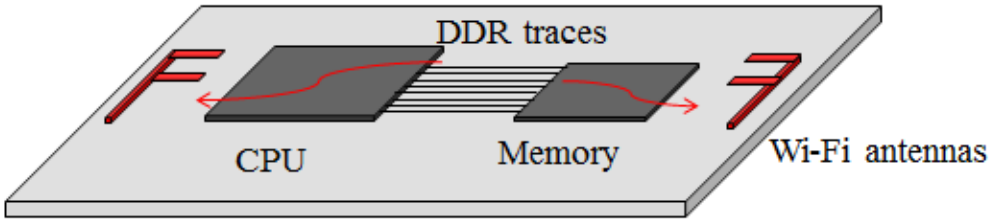

Figure 1. DUT illustration

First, near-field measurements of source and antenna are performed using electromagnetic (EM) scanner to understand the RFI radiation and coupling physics. Then, dipole moment based reciprocity method is utilized to propose RFI mitigation methods like movement and/or rotation of noise source. The theoretical derivations and steps to maximize RFI reductions for two antennas are also provided. Finally, the results of the final modified board with reduced RFI are presented. Comparisons of measured RFI reduction and theoretical RFI reduction for both antennas are also presented.

2. NOISE SOURCE AND ANTENNA CHARACTERIZATION

EM scanner with spectrum analyzer is a fast and convenient tool to measure near-field emissions from any radiating source. Using EM scanner, the near field distribution of noise sources (i.e., SoC and DDR3 interface) is measured. The measurement setup and a simple illustration are shown in Figure 2. During the measurement, the device was configured in stress mode to emulate high-speed data transfer between CPU and DDR3. The resonant-type H field probe at 2.45 GHz is used and scanning is done at channel 6 of Wi-Fi. The resolution band width (RBW) of spectrum analyzer is set to 100 KHz with a

sweep time of 50 ms. Average detector is used, and scan data is sampled using a max hold mode for 15 seconds. Further scanning area was chosen to be 30 mm × 30 mm with a 2 mm step.

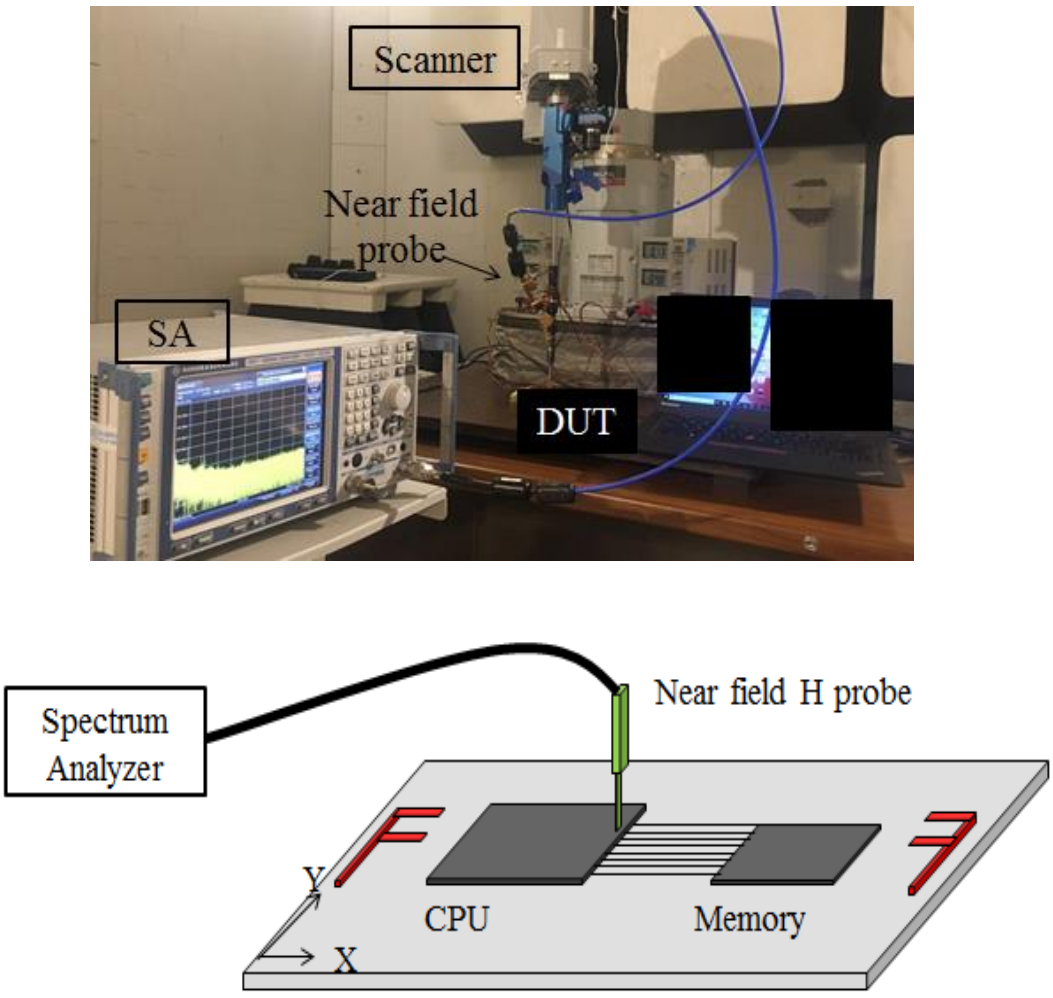

Figure 2. A photo of the measurement set-up with a simple illustration

The measured near-field patterns with H_x and H_y components are shown in Figure 3(a). The H field patterns are similar to the field patterns of a single magnetic dipole M_y. Similar patterns were observed in a cell phone [3]. Once the source dipole is

identified, the magnitude of the single magnetic dipole can be calculated using the least squares method with magnitude-only data [3]. Figure 3(b) shows the near-field patterns calculated from the reconstructed magnetic dipole. According to electromagnetics theory and analysis in [3], the pattern center is the location of the dipole moment. In the measured field patterns, the pattern center corresponds to the center of the microstrip lines as depicted in Figure 4. The reconstructed magnetic dipole M_y can be understood as an electric current loop in xz-plane facing y direction.

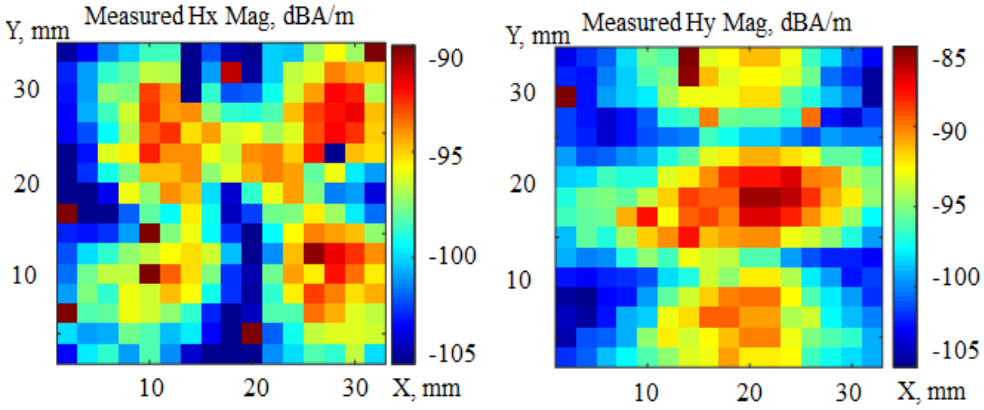

(a)

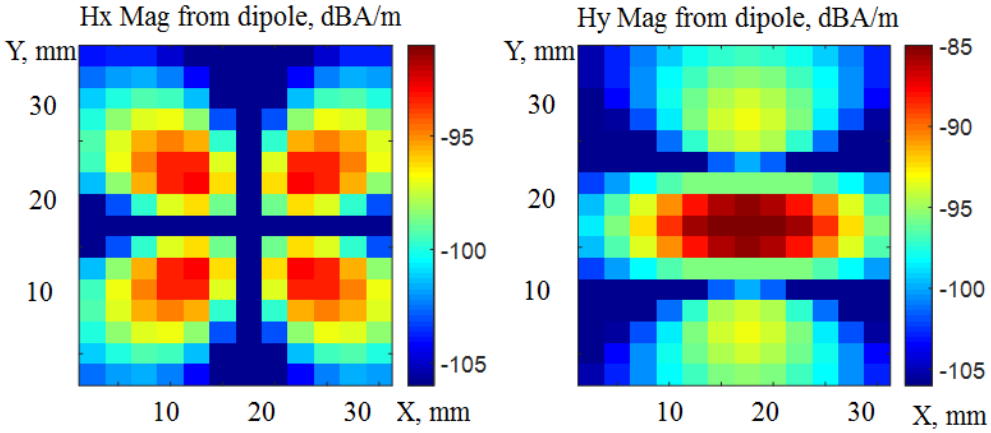

(b)

Figure 3. (a) Measured $|H_x|$ and $|H_y|$ (b) calculated $|H_x|$ and $|H_y|$ from the reconstructed magnetic dipole

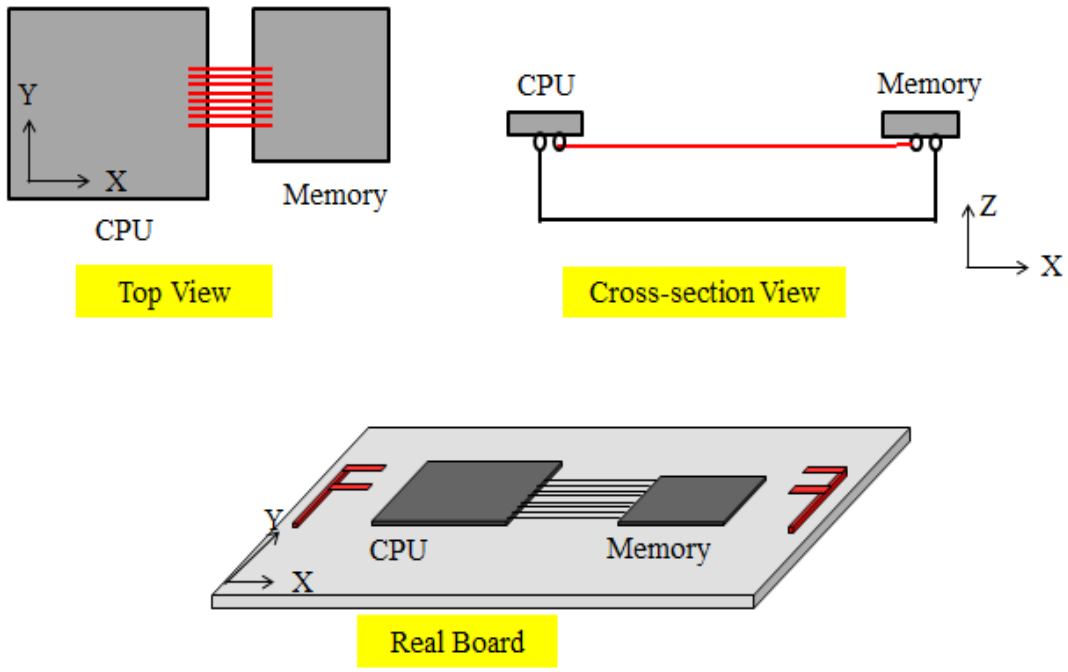

Figure 4. Routing between the CPU and memory IC

Since the radiation source is a single M_y dipole moment in the forward problem, according to [4], the coupled voltage to the victim antenna can be calculated by the following equation

$$U_{fwd} = \frac{Z_L}{2U_{rev}^{+}}\left[\vec{H}_{rev} \cdot \vec{M}_{fwd}\right] \tag{1}$$

where U_{fwd} is the coupled voltage at antenna port due to the noise source, M_{fwd} is the dipole moment in the forward problem (M_y in this device), Z_L is the load impedance (50 Ω), U_{rev}^{+} is the incident voltage from the antenna port in the reverse problem, H_{rev} is the H field in the reverse problem with incident voltage of U_{rev}^{+}.

The measurement set-up of the reverse problem is shown in Figure 5. Vector network analyzer (VNA) is used along with EM scanner instead of spectrum analyzer.

The victim antenna is excited using port 1, and port 2 is connected to the near-field probe of the EM scanner. With the noise source turned off, the near-field components of antenna are measured by capturing S_{21} from VNA. Using probe calibration factor (A/m/V), S_{21} (dB) is converted to H-field (dBA/m). The measured $|H_y|$ in the reverse problem is shown in Figure 6. In the scanning plane, it is observed there are hot spots and cold spots of antenna H-field. According to (1), smaller H_y can lead to smaller coupled voltage on the antenna port. Thus moving M_y dipole (the noise source) to the smallest H_y location can help in reducing RFI. However in this device, smallest H_y location is at the edge of the scanning plane, which is also the edge of the main logic board. If this change was applied, then CPU and memory ICs must be placed at the edge of board, which is not a practical layout change. While reducing the magnitude of forward M_y will yield similar results, the method to reduce the magnitude will lead to signal integrity issues discussed previously.

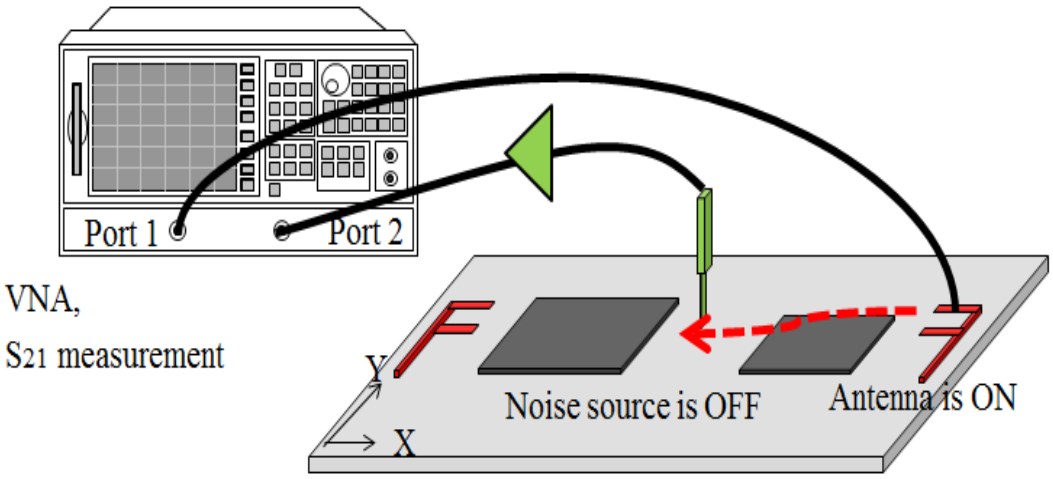

Figure 5. Measurement setup of the reverse problem with antenna excited

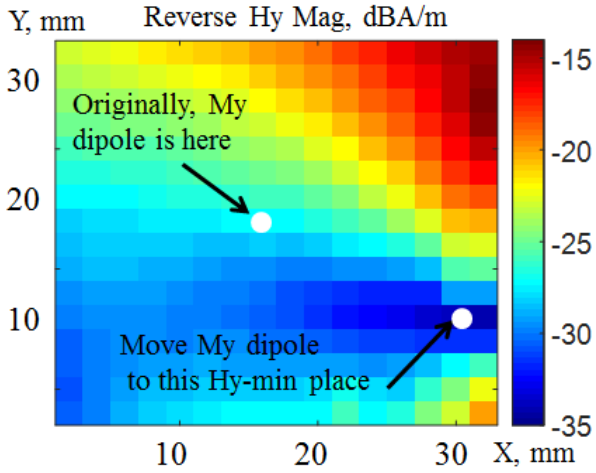

Figure 6. Measured $|H_y|$ in the reverse problem

3. RFI REDUCTION BY ROTATING NOISE SOURCE

In (1), it is worth noting that there is an inner product between two vectors: the noise source and reverse field ($\vec{H}_{rev}$ and $\vec{M}_{fwd}$). In this work, a novel method in manipulating the angle difference of two vectors is undertaken. With a certain angle, the inner product of these two vectors can be minimized. A general expression of $\vec{H}_{rev}$ and $\vec{M}_{fwd}$ is given as below

$$\begin{aligned} \vec{H}_{rev} &= \hat{x}\,|H_x|\,e^{i\theta_x} + \hat{y}\,|H_y|\,e^{i\theta_y} + \hat{z}\,|H_z|\,e^{i\theta_z} \\ \vec{M}_{fwd} &= \hat{x}\,|M|\,e^{i\theta_m}\cos\varphi + \hat{y}\,|M|\,e^{i\theta_m}\sin\varphi \end{aligned} \tag{2}$$

where $\hat{x}$, $\hat{y}$, and $\hat{z}$ are the unit vectors along x-, y- and z-axes, respectively. $|H_x|$ and θ_x is the magnitude and phase of the complex number H_x, respectively, which can be measured in the reverse problem. $|M|$ and θ_m are the magnitude and phase of the original M dipole,

respectively. φ is the rotation angle, relative to x-axis. Figure 7 shows a simple diagram of the rotation problem.

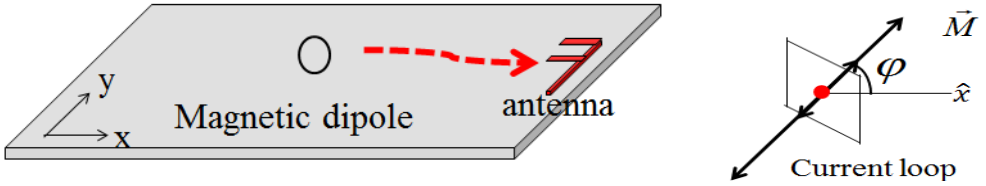

Figure 7. Simple diagram of the rotation problem

Substituting (2) into (1) and assuming U_{rev}^{+}=1 V, and Z_L=50 Ω, the coupled voltage can be obtained as below

$$\begin{aligned} U_{fwd} &= 25\vec{H}_{rev}\cdot\vec{M}_{fwd} = 25(\hat{x}\,|H_x|e^{i\theta_x}+\hat{y}\,|H_y|e^{i\theta_y}+\hat{z}\,|H_z|e^{i\theta_z})\cdot(\hat{x}\,|M|e^{i\theta_m}\cos\varphi+\hat{y}\,|M|e^{i\theta_m}\sin\varphi) \\ |U_{fwd}| &= 25\,|M|\sqrt{(|H_x|^2\cos^2\varphi+|H_y|^2\sin^2\varphi+2|H_x||H_y|\sin\varphi\cos\varphi(\cos\theta_x\cos\theta_y+\sin\theta_x\sin\theta_y)} \\ |U_{fwd}| &= 25\,|M_\varphi|\,|H_\varphi| \\ |H_\varphi| &= \sqrt{(|H_x|^2\cos^2\varphi+|H_y|^2\sin^2\varphi+2|H_x||H_y|\sin\varphi\cos\varphi(\cos\theta_x\cos\theta_y+\sin\theta_x\sin\theta_y)} \end{aligned} \tag{3}$$

where $|M_\varphi|$ is the magnitude of the magnetic dipole after rotation angle φ in xy-plane; $|M_\varphi|$ remains the same for any rotation angle φ in xy-plane. A special case for this rotation problem is that the reverse H field is linearly polarized. Namely, the phase difference between reverse H_x and H_y fulfills the relationship such that $\theta_x-\theta_y=\pm n\pi$. Then it leads to $\cos\theta_x\cos\theta_y+\sin\theta_x\sin\theta_y=\pm1$. In this special case, (3) is simplified as

$$\begin{aligned} |U_{fwd}| &= 25\,|M|\,(|H_x|\cos\varphi\pm|H_y|\sin\varphi) \\ |U_{fwd}| &= 25\,|M_\varphi|\,|H_\varphi| \\ H_\varphi &= (|H_x|\cos\varphi\pm|H_y|\sin\varphi) \\ &= (\hat{x}\,|H_x|\pm\hat{y}\,|H_y|)\cdot(\hat{x}\cos\varphi+\hat{y}\sin\varphi) \end{aligned} \tag{4}$$

In (4), H_φ is actually an inner product of two vectors, both of which are real numbers. In contrast, (1) is also an inner product of two vectors, both of which, however, are complex numbers. (1) depicts a general case ($\theta_x - \theta_y \neq \pm n\pi$), while (4) shows the special case ($\theta_x - \theta_y = \pm n\pi$). A simple diagram is drawn in Figure 8 to illustrate the special case ($\theta_x - \theta_y = \pm n\pi$). In Figure 8, when the loop is placed along the reverse H field line, there are no H field lines penetrating through the current loop. Thus, the inner product between the H field vector and the normal vector of the loop is zero and no noise coupling occurs. The worst RFI for the linearly polarized case happens when the H field vector is perpendicular to the current loop. Another diagram is drawn in Figure 9 to illustrate the general case ($\theta_x - \theta_y \neq \pm n\pi$). In Figure 9, when the loop is placed along the longer axis of the ellipse, there are less H field lines penetrating through the current loop. Thus, the inner product between the H field vector and the normal vector of the loop becomes the minimum. The worst RFI for the elliptically polarized case happens when the H field vector is placed along the shorter axis. There are more H field lines penetrating through the current loop. Thus, the inner product between the H field vector and the normal direction of the loop becomes the maximum.

Taking one of the Wi-Fi antennas on this board for analysis (right-side antenna), the magnitude and phase of reverse H_x and H_y is obtained from the reserve problem measurement. The measured phase difference of reverse H_x and H_y is 181˚, which is very close to the special case in Figure 8 (a linearly polarized reverse H field has phase difference of 180˚ or 0˚). It is expected that RFI will be minimum at a certain rotation angle. By substituting magnitude and phase of reverse H_x and H_y into (3), coupled voltage at any rotation angle φ is obtained. The theoretical RFI reduction is defined by

subtracting the coupled voltage at any rotation angle φ from the original coupled voltage where dipole moment is M_y (where φ is 90˚).

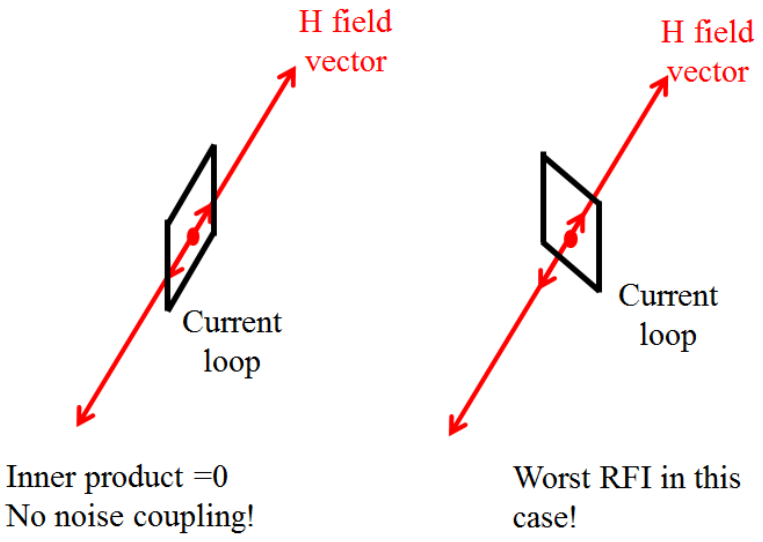

Figure 8. A special case for the rotation problem: Reverse H field is linearly polarized ($\theta_x - \theta_y = \pm n\pi$).

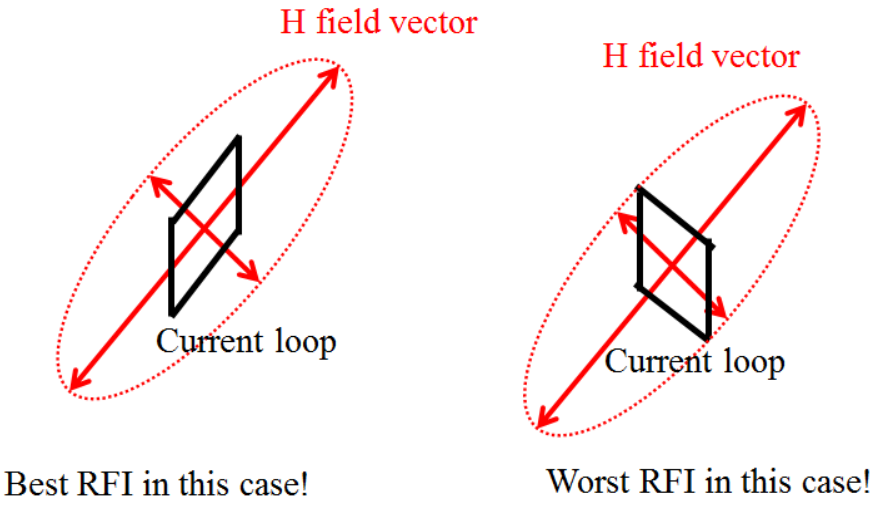

Figure 9. A general case for the rotation problem: Reverse H field is elliptically polarized ($\theta_x - \theta_y \neq \pm n\pi$)

As stated above $|M_\varphi|$ stays the same for any rotation angle φ in xy-plane. The RFI reduction is from the reduction in $|H_\varphi|$ compared to original $|H_y|$ (namely φ=90˚). Measurement is also done to show the reduction in $|H_\varphi|$ using the setup shown in Figure 5. The baseline was set as measured $|H_y|$ when the probe is facing y direction. For any other rotation angle φ, the probe will be rotated to measure $|H_\varphi|$. The measured reduction in $|H_\varphi|$ is defined by subtracting the $|H_\varphi|$ at any rotation angle φ from the original $|H_y|$.

Measured and theoretical RFI reduction for any rotation angle φ is shown in Figure 10. A good agreement seen between measurement and theory validates the proposed methodology. When the rotation angle is 27˚, maximum RFI reduction is achieved to be 38.8 dB. In simulation, the RFI between the original case and the φ =27˚ rotation case are compared. Simulation results are shown in Figure 11. Simulated RFI reduction is 38 dB, which agrees with the measured and theoretical RFI reduction very well.

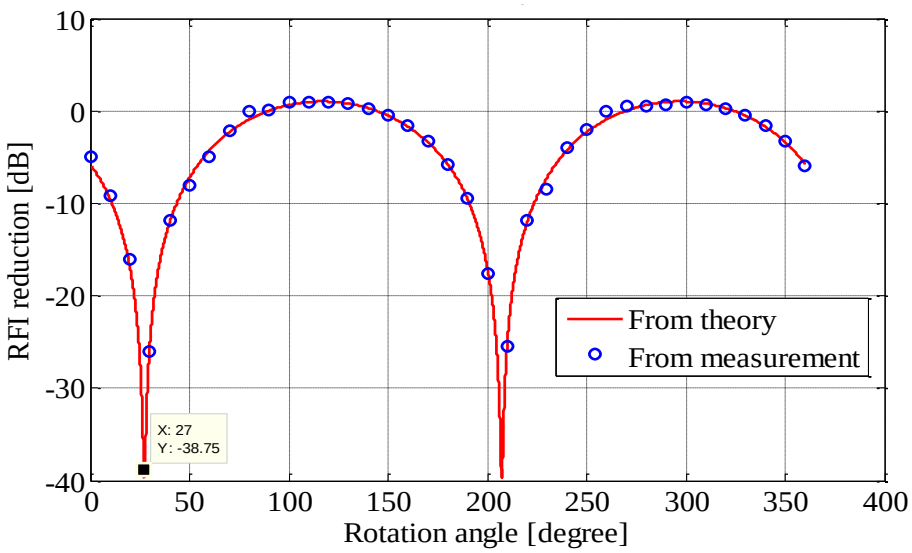

Figure 10. Theoretical and measured RFI reduction for various rotation angle φ

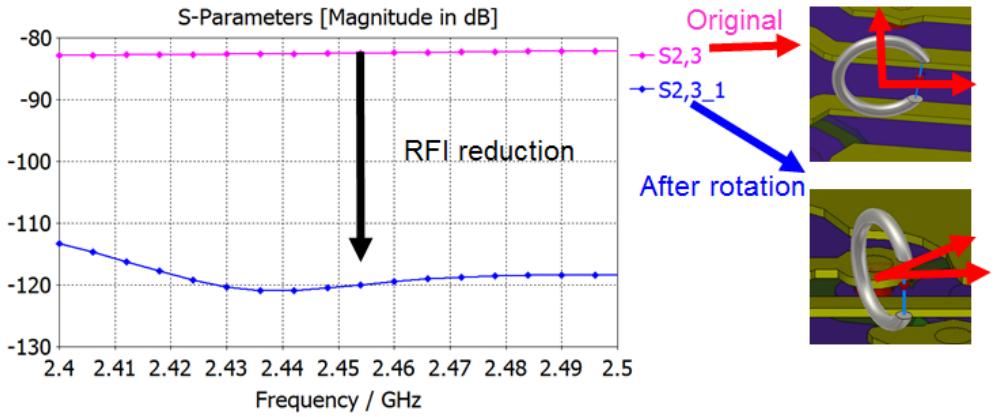

Figure 11. RFI reduction in simulation between φ=90˚ (original case) and φ=27˚ (best rotation angle)

4. RFI REDUCTION FOR TWO ANTENNAS

As In the previous sections, a theoretical way to improve RFI without impacting signal integrity and adding cost to the product is introduced. Simulations and measurements show that rotating the magnetic dipole moment, which is the noise source, to φ=27˚ can significantly reduce RFI for one of the selected Wi-Fi antenna on this device (the right-side antenna). However, in an actual device, the two antennas (for MIMO functionality) need to be improved together. Two special cases are studied for the two-antenna system. The first special case is that the two antennas are symmetrical around the y-axis. The second special case is that the two antennas are symmetrical to source point of magnetic dipole moment. Let us assume that the near field is a general case, i.e. elliptically polarized. Then, for the y-symmetry case in Figure 12(a), the best angles for RFI reduction are achieved at different angles, as denoted by the two different shorter axes of the two ellipses. In other words, there is no best angle to achieve

maximum RFI reduction for both antennas. In contrast, for the point symmetry case in Figure 12(b), the best angles for RFI reduction on both antennas is achieved along the same line, as denoted by the shorter axes of the same ellipse. For the first special case in Figure 12(a), where two antennas are symmetrical around the y-axis, the theoretical RFI reduction can be calculated by taking the simulated magnitude and phase of H_x and H_y of both antennas into (3). The theoretical RFI reductions for both antennas are shown in Figure 13(a). The best angle to achieve maximum RFI reduction for right-side antenna and left-side antenna is φ=27˚ and φ=153˚, respectively. In this y-symmetry case, there is no best angle to achieve maximum RFI reduction for both antennas. On the contrary, for the point-symmetry case in Figure 12(b), there is a best angle φ=27˚ to achieve maximum RFI reductions for both antennas, as shown in Figure 13(b).

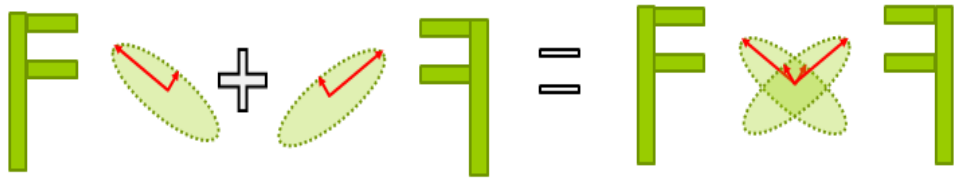

(a)

(b)

Figure 12. RFI reduction diagram for two antennas; (a) Both antennas are symmetrical over y-axis (b) Both antennas are symmetrical over the dipole moment source point

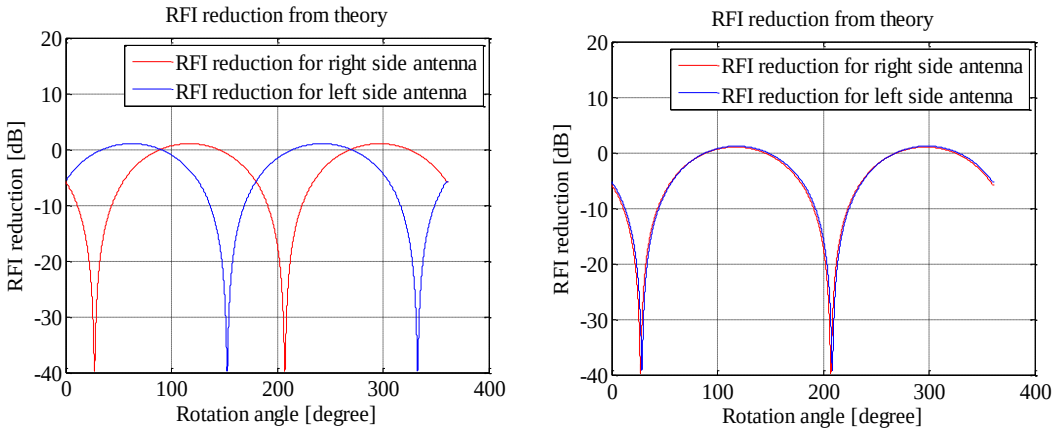

Figure 13. Theoretical RFI reduction at any rotation angle φ for two antennas: (a) both antennas are symmetrical over Y axis; (b) Both antennas are symmetrical over the dipole moment source point

However, due to the limitation of the layout space on this board, it was difficult to rotate the dipole moment to φ=27˚ while keeping the dipole location the same and keeping two antenna point symmetrical over the dipole moment source. So the ideal case in Figure 13(b) was not feasible in the real board design. In the final modified layout, the locations of the noise source were moved up 3 mm in order to accommodate the placement of other components. Because of the movement of 3 mm, for the right-side antenna, the phase difference of reverse H_x and H_y at the new location is 153˚, which is worse than the linearly polarized case in original location(phase difference of reverse H_x and H_y is 181˚). It's expected that the RFI reduction in this new location will not be as good as 38 dB for the original location (181˚ as the phase difference). Figure14 shows the comparisons between the original board and the final modification board. Based on the simulated reverse-field distribution of two antennas, the theoretical RFI reduction for any rotation angle φ is shown in Figure 15. When the rotation angle φ is 27˚, the theoretical

RFI reduction for the left and right side antennas are 6.5 dB and 9 dB. It's a compromise to achieve good RFI reductions on both antennas and also take care of other component placements.

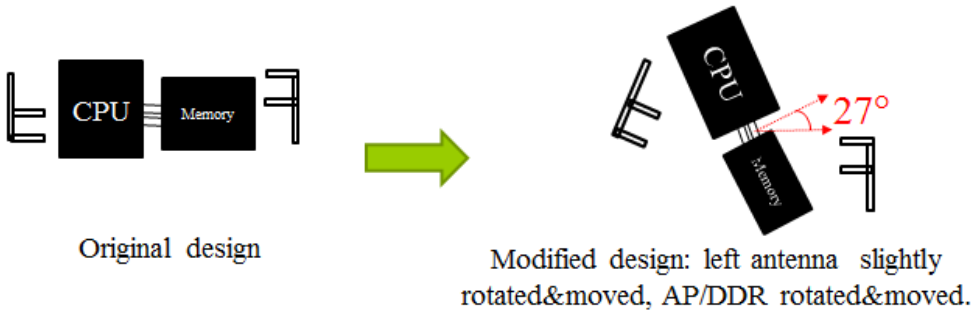

Figure 14. The original design and the modified design

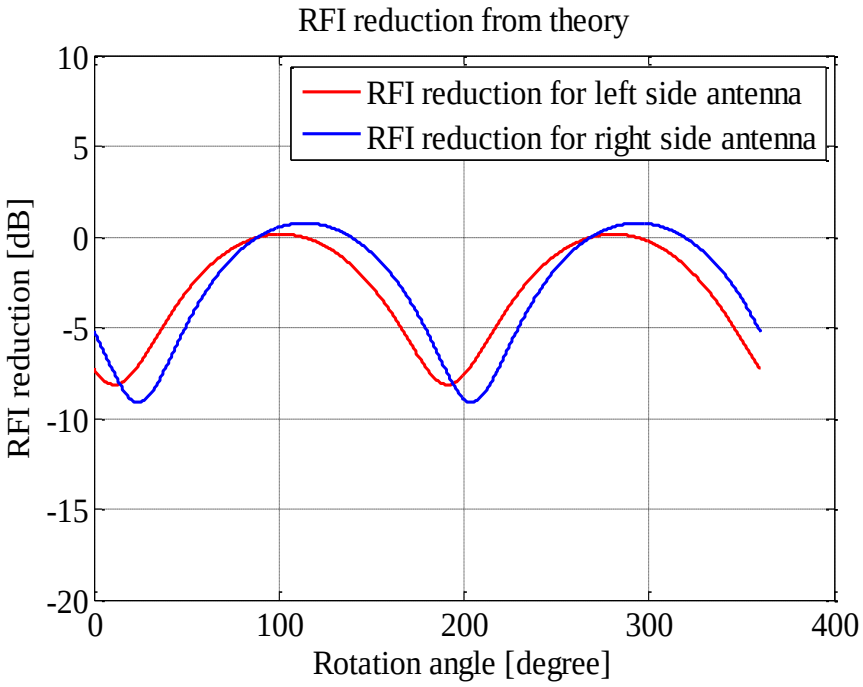

Figure 15. The theoretical RFI reduction at any rotation angle φ for the two antennas on the modified board

The device with the new placement has been fabricated and measured. The measured RFI for the right-side antenna between the modified design and the original design is shown in Figure 16. The measured RFI reduction for the left-side antenna is 4 dB and for the right-side antenna is 8 dB at 2.437 GHz (channel 6 of 2.4 GHz Wi-Fi). The RFI reductions for both antennas agree well with the theoretical RFI reduction. The error is within 2.5 dB. Overall, good RFI reduction is achieved for both antennas. The proposed RFI reduction methodology is validated successfully.

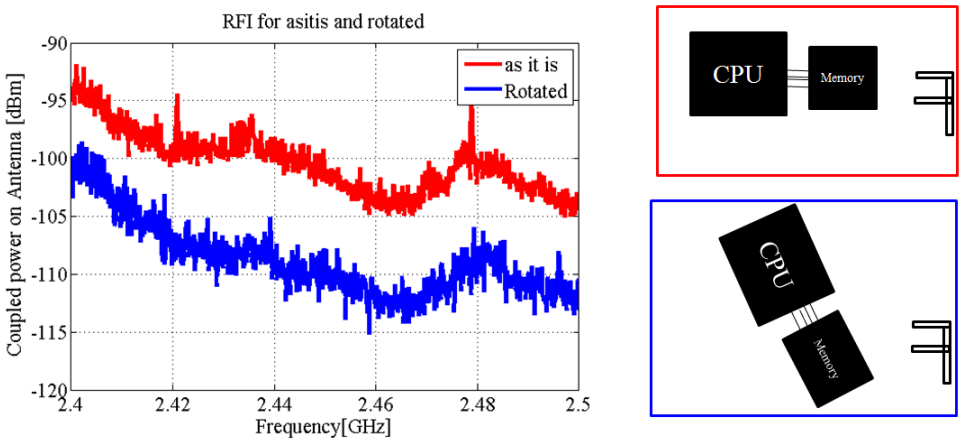

Figure 16. Measured RFI reduction for the right-side antenna between the modified design and the original design

5. CONCLUSION

RFI reduction for a real consumer electronic device is studied. Considering the layout limitation of the product, the proposed RFI mitigation involves rotating the CPU and DDR chip by a certain angle without compromising signal integrity. In addition to retaining signal integrity, the proposed method doesn't require shield can to meet RFI

specification for achieving the desired Wi-Fi performance. New boards with the suggested changes were manufactured, and measured results showed a good RFI reduction (up to 8 dB) compared to the original board. The measured RFI reduction has a good agreement with theoretical RFI reduction. The proposed method enables a new dimension to RFI mitigation with cost-saving opportunities.

REFERENCES

[1] Y. Wang et al., “A Simulation-Based Coupling Path Characterization to Facilitate Desense Design and Debugging,” in Proc. of IEEE Symp. Electromagn.Compat., 2018, pp. 150-155.

[2] Q. Huang et al., “Desense Prediction and Mitigation from DDR Noise Source,” in Proc. of IEEE Symp. Electromagn.Compat., 2018, pp. 139-144.

[3] Q. Huang, F. Zhang, T. Enomoto, J. Maeshima, K. Araki and C. Hwang, "Physics-based dipole moment source reconstruction for RFI on a practical cellphone", IEEE Trans. Electromagn. Compat., vol. 59, no. 6, pp. 1693-1700, Dec. 2017.

[4] Q. Huang, T. Enomoto, S. Seto, K. Araki, J. Fan and C. Hwang “Accurate and Fast RFI Prediction Based on Dipole Moment Sources and Reciprocity” in Proc. of DesignCon, 2018.

III. MACHINE LEARNING BASED SOURCE RECONSTRUCTION FOR RF DESENSE

ABSTRACT

In radio frequency interference study, equivalent dipole moments are widely used to reconstruct real radiation noise sources. Previous reconstruction methods, such as least square method (LSQ) and optimization method are affected by parameter selections, such as number and locations of dipole moments and choices of initial values. In this paper, a new machine learning based source reconstruction method is developed to extract the equivalent dipole moments more accurately and reliably. Based on the near field patterns, the proposed method can determine the minimal number of dipole moments and their corresponding locations. Further the magnitude and phase for each dipole moment can be extracted. The proposed method can extract the dominant dipole moments for the unknown noise sources one by one. The proposed method is applied to a few theoretical examples first. The measurement validation using a test board and a practical cellphone are also given. Compared to the conventional LSQ method, the proposed machine learning based method is believed to have a better accuracy. Also, it's more reliable in handling noise in practical applications.

1. INTRODUCTION

Modern connected electronic devices typically have multiple radio frequency (RF) antennas. For example, today's cellphones have multiple antennas to offer connectivity

covering Wi-Fi, Bluetooth, global positioning system (GPS), global system for mobile communication(GSM), and several long-term evolution (LTE) bands. Together, all of these antennas cover a relatively wide frequency range. Other trends for electronics include shrinking device sizes and increasing clock speeds and data rates. Many components within a cellphone, such as the display module, camera module, and CPU chips, can radiate and potentially couple to one of the many RF antennas [1]. These unintentional noise sources might radiate in a broad frequency band, so it is highly possible that the noise spectrum falls into the frequency range of the multiple RF antennas. Also, RF antennas often have high sensitivities to ensure high speed data communications. Even weak radiation from an unintentional noise source can be picked up by the RF antennas. This unintentional coupling to the RF antennas degrades the sensitivity of the antennas. This problem is known as RF desense. An illustration of this problem is shown in Figure 1. To understand the desense issue, the first step is to identify the noise sources and obtain accurate models of the noise sources. The most straightforward method is to model the whole problem directly using full wave simulation. However, this direct simulation often takes a long time. If a certain change is made during debugging, another round of full wave simulation is needed. Further, noise sources like integrated circuits (ICs) are typically quite difficult to model due to their complexity. Design engineers don't always have the access the exact geometrical details of an IC due to intellectual property protection from IC companies. Thus, the direct simulation is often not the best choice.

Recently, many efforts have been focused on equivalent dipole moment modeling for radiation sources [2]-[4]. An array of electric and magnetic dipole moments is used to

replace the radiation source, based on near field scanning measurements. The extracted dipole moments are relatively easy to import into full wave simulation tools [4]. If designers have both the equivalent dipole moment source model and the 3D model of victim antenna, the rest of the coupling problem can be done using full wave simulation. So the key is to obtain an accurate equivalent model for the real noise source. Previously a uniform array of electric and magnetic dipole moments is pre-defined to replace the noise source. The Least Square Method (LSQ) is then used to solve the magnitude and phase of each dipole moment. However, this method is prone to measurement noise of the near field data which is inevitable in near field scanning experiments. In particular, when the number of dipole moments is large, the solution from the LSQ method may be non-physical. Although a non-physical solution can match the field well at the scanning plane, it fails to predict the fields well at other locations [4]. In [5] and [6], optimization algorithms are used. The performance of the optimization algorithms depends heavily on the initial value. The optimization algorithms will fail if a bad initial value is chosen. A more reliable method is needed to reconstruct equivalent dipole moments accurately and also with physical meanings.

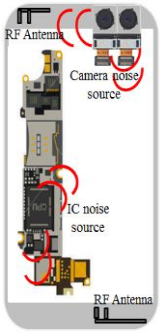

Figure 1. RF antennas and noise sources inside a cellphone

Although the described problem is encompassed within the field of electromagnetics, it is beneficial to look at the problem from another perspective. The objective of the problem is to extract information (equivalent dipole moment sources) from near field plots. This is very similar to a typical computer vision problem, where computers attempt to extract information from images or videos. For example, in Figure 2(a), the image contains a table and a chair. After adequate training, machine learning algorithms are able to identify both the chair and the table. In a similar fashion, algorithms can be trained to identify the dominant dipole moments from near field plots. A typical near field pattern for a cell phone is shown in Figure 2(b).

(a) (b)

Figure 2. Similarities between a typical computer vision problem and the source reconstruction problem: (a) A table and a chair can be indentified in the picture. (b) Dipole moment sources need to be extracted from the near field plot of a cellphone

In this paper, a machine learning algorithm is developed using a training set consisting of the field patterns for the six basic dipole moments. After the training, the algorithm is capable of extracting the primary dipole moment from more complicated field patterns. Once the type of dipole moment is identified, the location of the dipole moment is further determined using autocorrelation. The least square method is used to

extract the magnitude and phase for this dominant dipole moment. After the first and most dominant dipole moment is extracted, a new field pattern is generated by subtracting the field pattern of the first dipole moment from the original field pattern. The same process is repeated on the newly obtained field pattern. The iteration stops when the difference between the field pattern from the extracted dipole moments and the field pattern from the measurement meets a certain criterion or a maximum iteration number reaches. In this way, the most dominant dipole moments for the complex noise source can be extracted one by one. The proposed method is applied to a few theoretical examples first. The measurement validations using a test board and a practical cellphone are also given.

2. MACHINE LEARNING BASED SOURCE RECOSNTRUCTION

Dipole moments are the most basic radiation sources. The electric dipole moment consists of an infinitely small electric current segment, denoted as a P dipole moment. By duality, a magnetic dipole moment is an infinitely small magnetic current segment, denoted as an M dipole moment. An infinitely small magnetic current segment is actually an infinitely small electric current loop. For a magnetic dipole moment, the direction is defined as the perpendicular direction to the plane of the electric current loop. For example, an Mx dipole moment denotes the magnetic current going towards the x-direction, or the electric current loop in the yz plane. Based on orientations, there are six types of basic dipole moments, as shown in Figure 3. For the basic dipole moments, the near and far fields can be calculated from the analytical formulas given in [4]. Thus, the

field patterns above the noise source can be analytically calculated. The goal is to obtain a field pattern database from the six basic dipole moments. The machine learning algorithm is trained by these field patterns. In order to mimic the noise in real measurements, different amounts of small random noise are added to the ideal dipole moments. For example, the Hx patterns for the magnetic dipole My are shown in Figure 4. Clearly, every field pattern is different because of the added random noise. However, the overall shape of the pattern is the same butterfly shape. The butterfly shape is the key feature in identifying the My dipole moment. The whole training set is formed by 600 field patterns from the six types of basic dipole moments.

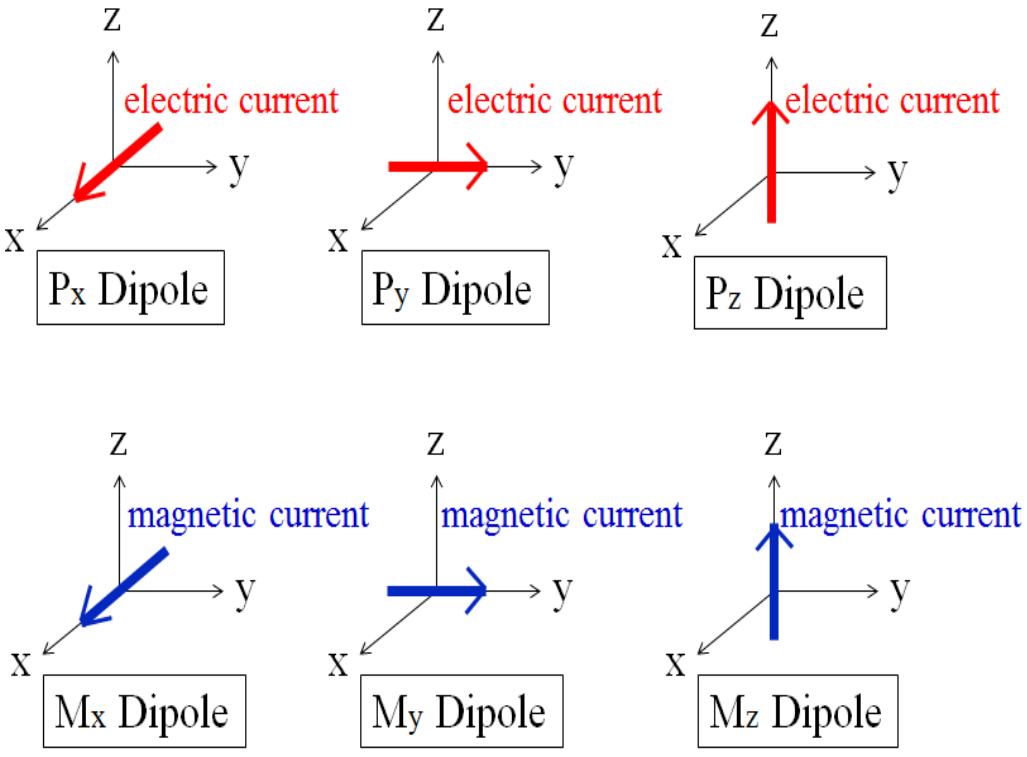

Figure 3. Six types of basic dipole moment sources

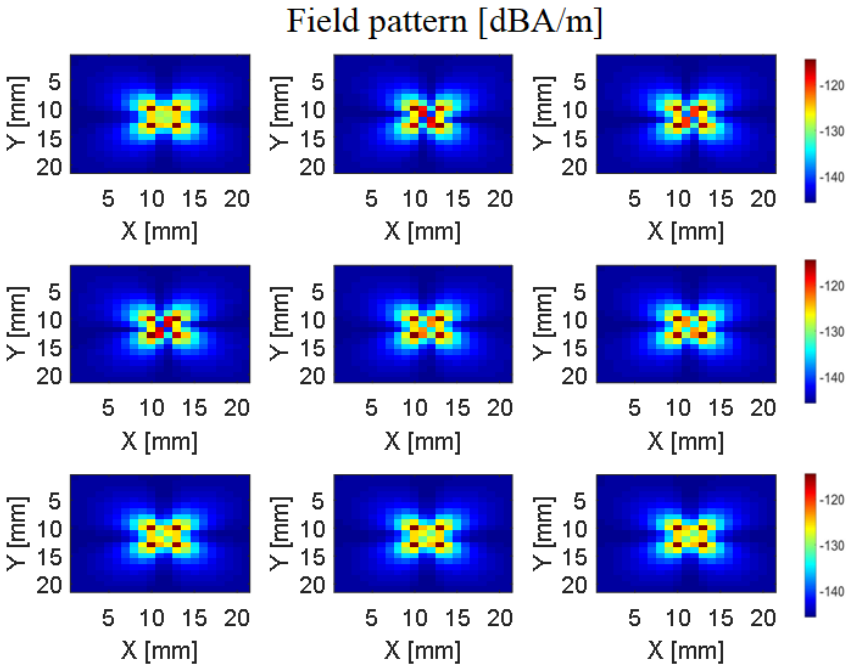

Figure 4. H_x field patterns for M_y dipole moment with random noise added

Different types of dipole moments have different field patterns. Local features of the field pattern are used to classify the dipole moment type. In computer vision, local features are compact vector representations of a local neighborhood inside a picture and are the building blocks of many computer vision algorithms. In this study, a histogram of oriented gradients (HOG) is used to extract the local features from different field patterns. According to [7], HOG provides an excellent performance for human detection. HOG is therefore expected to be sufficient enough to extract the local features of field patterns in this work. Figure 5 shows a field pattern and its corresponding HOG features. In machine learning, support vector machine (SVM) is a type of supervised learning used for classification analysis. In this work, given a set of training field patterns, each field pattern is marked as belonging to one dipole moment category. The SVM algorithm is trained by those field patterns and its corresponding category.

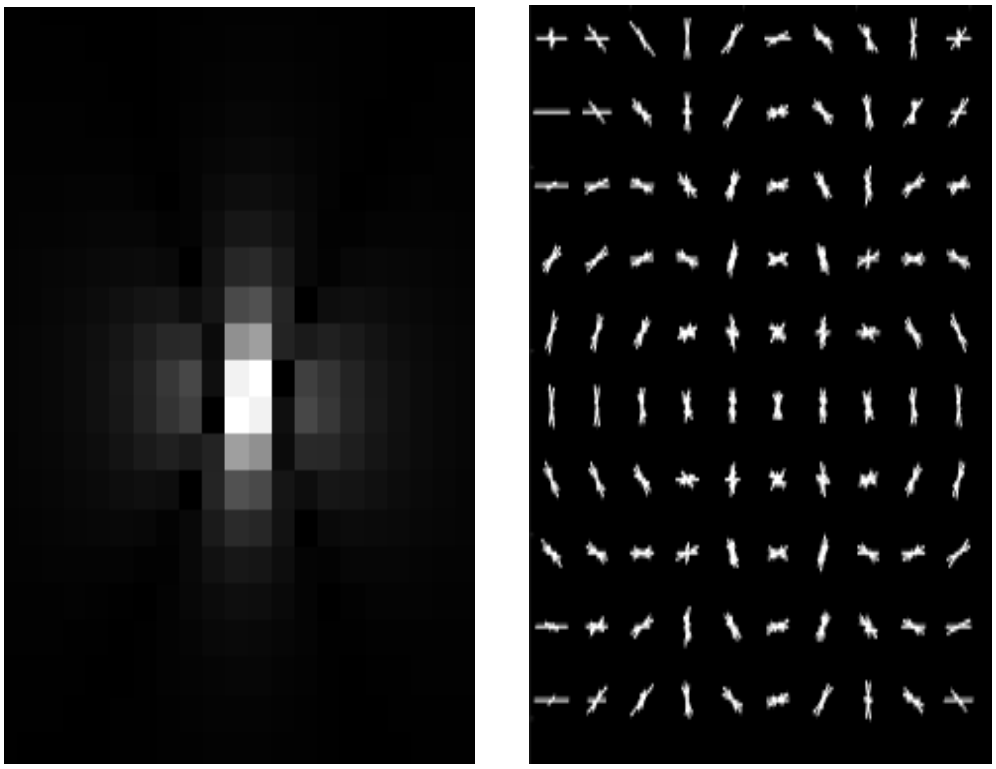

(a) (b)

Figure 5. (a) A field pattern from the training database, (b) HOG features

After the training, the algorithm will be able to identify the main dipole moment for complicated field patterns. The workflow of the machine learning algorithm is shown in Figure 6. After the validated machine learning algorithm is obtained, it's utilized to extract equivalent dipole moments, one by one, from an unknown field pattern. The workflow is shown in Figure 7. Firstly, the unknown field pattern is represented with HOG features. Then the validated machine learning algorithm will determine the dominant type of dipole moment in this unknown field pattern. Once the type of the dominant dipole moment is identified, the autocorrelation between the unknown field pattern and the field pattern of the dominant dipole moment is used to identify the location of the dipole moment.

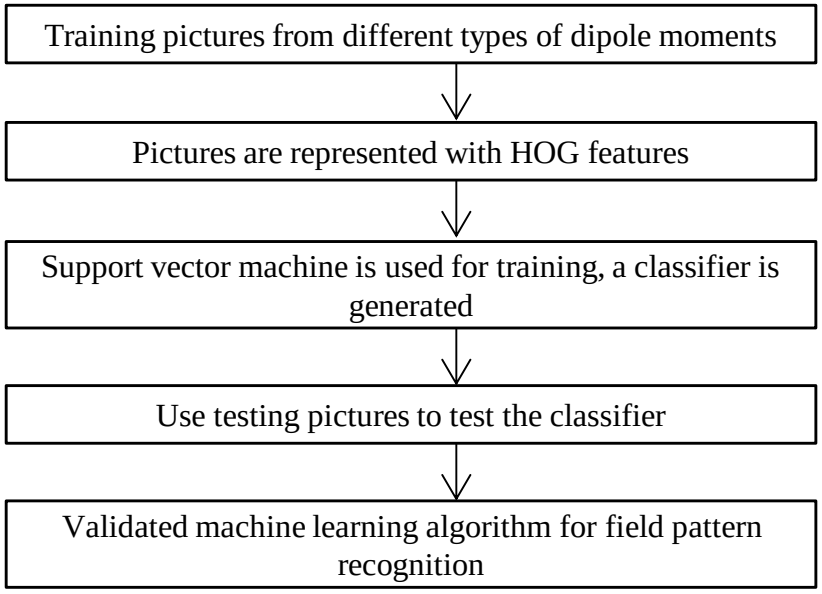

Figure 6. Workflow of machine learning algorithm

After the type and location of the most dominant dipole moment is determined, LSQ is used to find the magnitude and phase. Because there is only one dipole in this LSQ method, the issues of overfitting in the conventional LSQ method is intelligently solved here. In this way, the first and most dominant dipole moment for the unknown noise source is successfully obtained. The error between the unknown field and the field of the dominant dipole moment is further calculated. If the error is smaller than the defined criteria, the process will end. It means that the unknown noise source contains only one dominant dipole moment. However, if the error is larger than a certain criteria, it means that the dominant dipole moment cannot sufficiently represent the unknown noise source. In this case, a new field pattern is obtained by subtracting the field of the dipole moment from the original field pattern. The new field pattern goes through the whole process again to obtain the second dominant dipole moment source. In this way, the most dominant dipole moments can be extracted one by one.

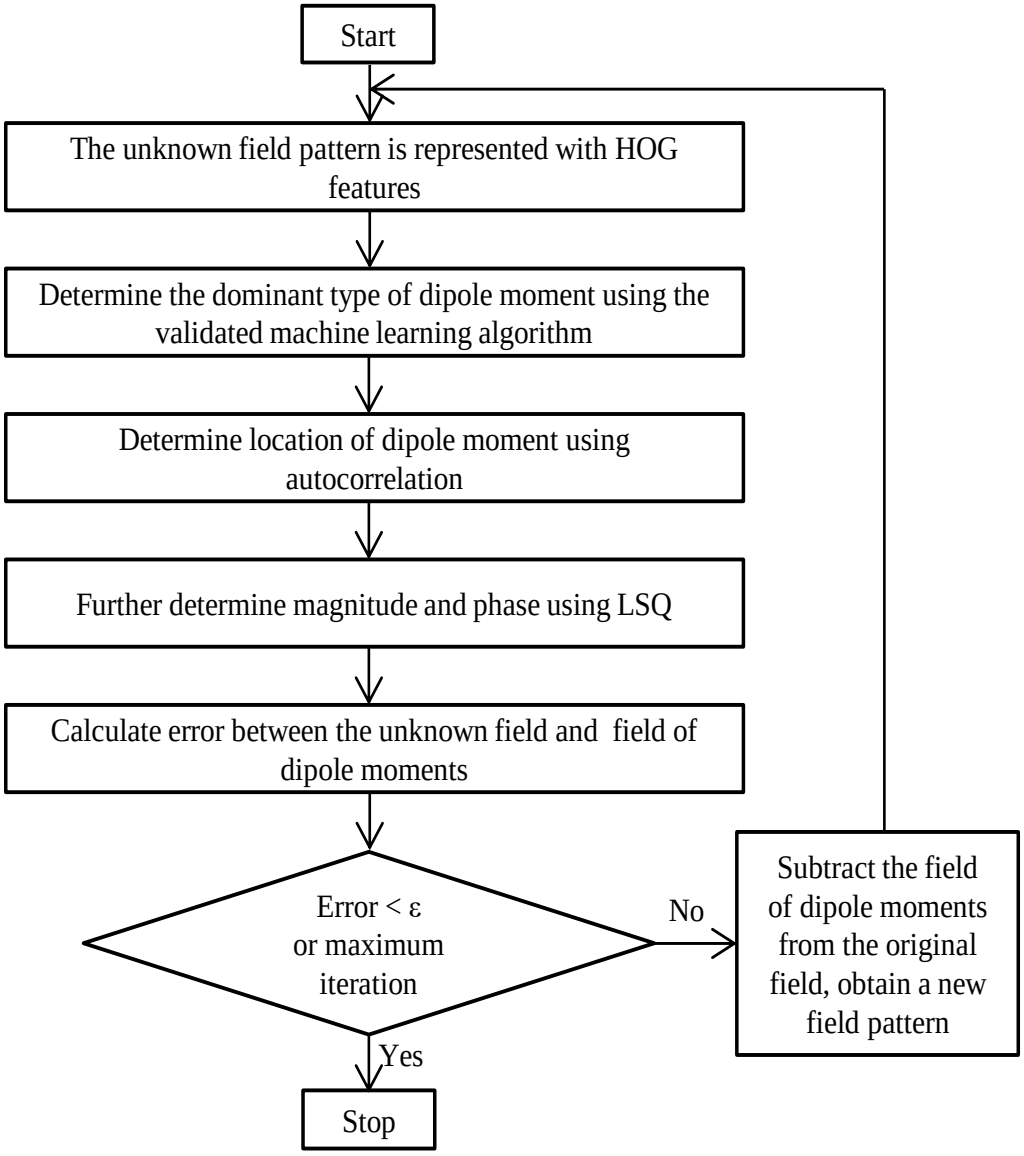

Figure 7. Workflow of machine learning based dipole moment extraction

3. VALIDATIONS

Two theoretical examples are discussed below to validate the proposed method. The first theoretical example is shown in Figure 8. For an unknown noise source, the near field patterns of H_x and H_y are provided. Using the traditional method of mapping hot

spots, there are at least 7-8 radiation sources. In later discussion, this claim is shown to be incorrect. In comparison, the proposed machine learning method can provide the correct source reconstruction. It can also generate the minimum number of dipole moments for this unknown noise source. The detailed dipole moment extracting procedure is shown in Figure 9. For the given input field pattern, the algorithm will first find the maximum field position and pick out the nearby field based on a certain threshold. Using this process, the first pattern is cut out from the original field pattern. The first pattern is sent to the pre-trained machine learning algorithm. The machine learning algorithm determines the type of the dipole moment. After the type of dipole moment is determined, the location of the dipole moment is further determined using autocorrelation.

The LSQ method is used to solve the magnitude and phase of the first dipole moment. In this way, the first and most dominant dipole moment is extracted. The field for the extracted dipole moment is then subtracted from the original field pattern, resulting in a new field pattern. The dipole extraction and field subtraction procedure is repeated on this new field pattern until a certain error criteria is reached. The original field pattern can be well represented by the extracted dipole moments. The tangential H field from the most dominant dipole moment M_x and the second most dominant dipole moment M_y is shown in Figure 10 (a) and (b). For the unknown noise source in Figure 8, it turns out that there are two dominant dipole moments inside the source. The most dominant dipole is an M_x dipole. The second dominant dipole is a M_y dipole. Using the proposed source reconstruction method, the two dipole moments can be extracted, along with the corresponding magnitude and phase.

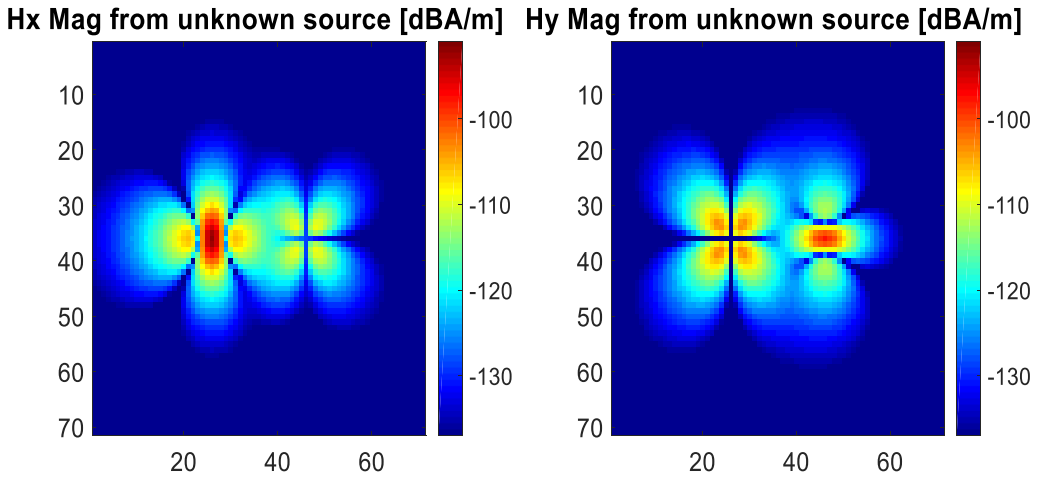

Figure 8. Field patterns of H_x and H_y for an unknown noise source

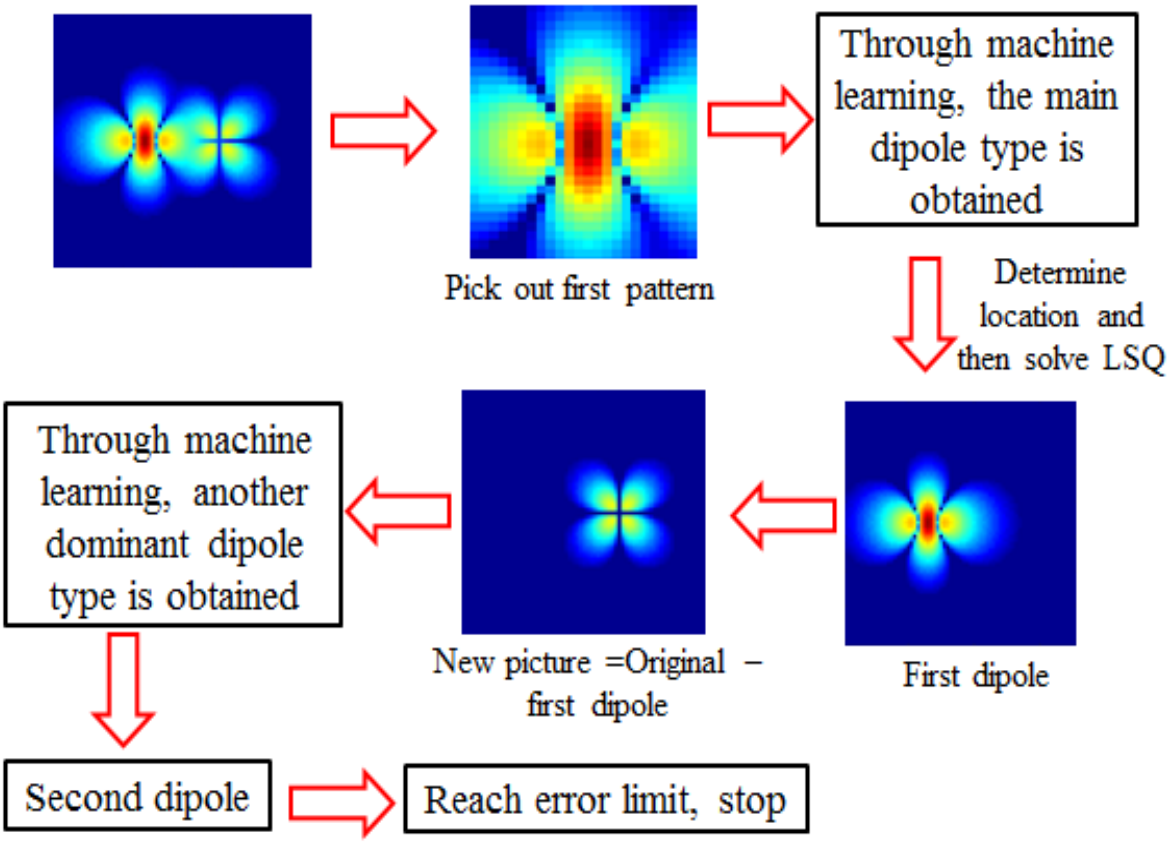

Figure 9. Workflow of the machine learning based source reconstruction on the unknown source in Figure 8

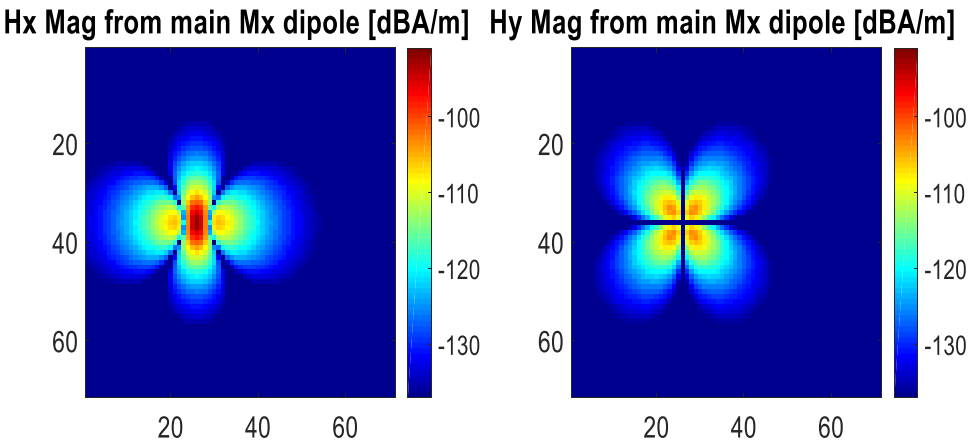

(a)

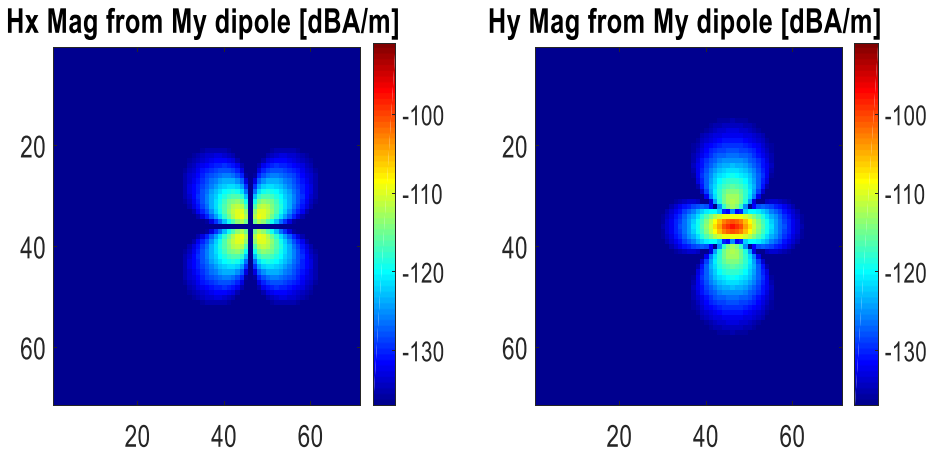

(b)

Figure 10. H_x and H_y patterns from the extracted dipole moments: (a) Magnitude of H_x and H_y from the most dominant dipole moment M_x. (b) Magnitude of H_x and H_y from the second most dominant dipole moment M_y

Because the two dipole moment sources in Figure 8 are located sufficiently far away, the two field patterns are relatively recognizable. A second theoretical example with a more complex pattern is also provided to demonstrate the robustness of the proposed method. The field pattern for an unknown noise source is shown in Figure 11. The patterns in Figure 11 cannot be easily recognized. The machine learning based

source reconstruction method can still work correctly. The workflow is shown in Figure 12. For the unknown noise source in Figure 11, it turns out that there are two dominant dipole moments inside the source. The most dominant dipole is a M_y dipole moment, which is extracted out first by the algorithm. The second most dominant dipole is a M_x dipole moment. These two dipole moments are located at the same place. Compared to the field pattern of Figure 8, this is more complex, because the near field is affected by the magnitude and phase of these two dipole moments. This is also the reason that the field patterns are not easily recognized. Using the proposed source reconstruction method, the two dipoles can be successfully extracted with the correct magnitude and phase. Figure 13 shows the field patterns from these two dipole moments. It is worthwhile to mention that phase information of the near field is needed here if two dipole moments are close. Without phase information of the near field, the two closely placed dipole moments cannot be correctly separately.

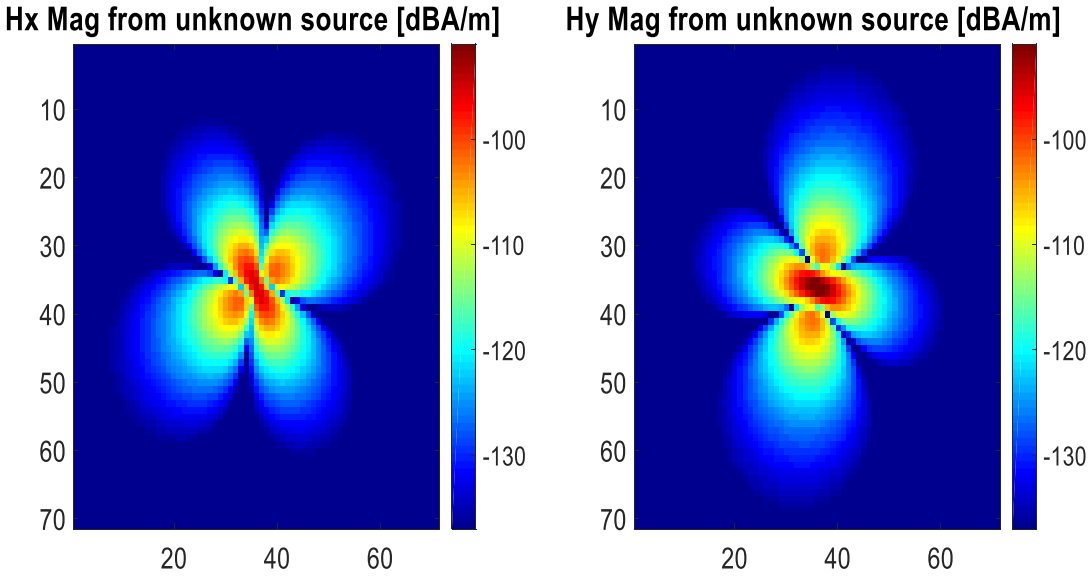

Figure 11. Field patterns of Hx and Hy for another unknown noise source

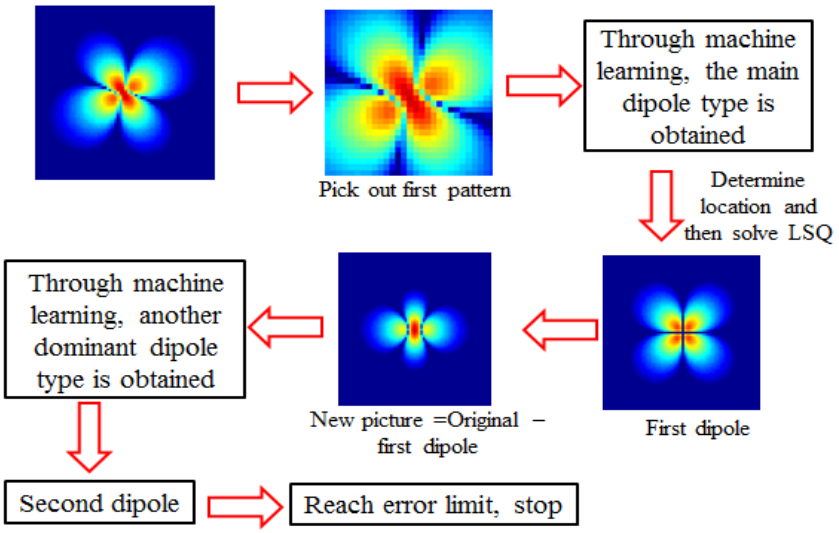

Figure 12. Workflow of the machine learning based source reconstruction on the unknown source in Figure 11

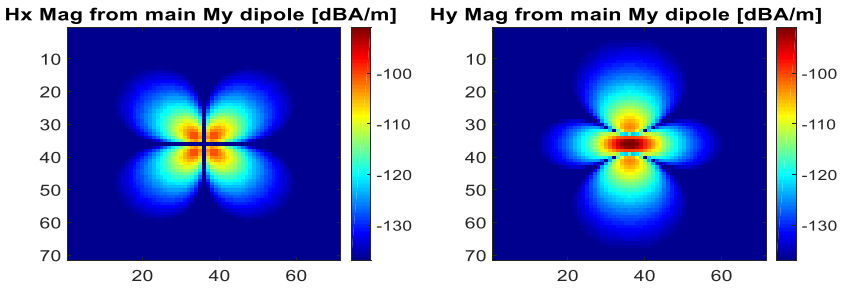

(a)

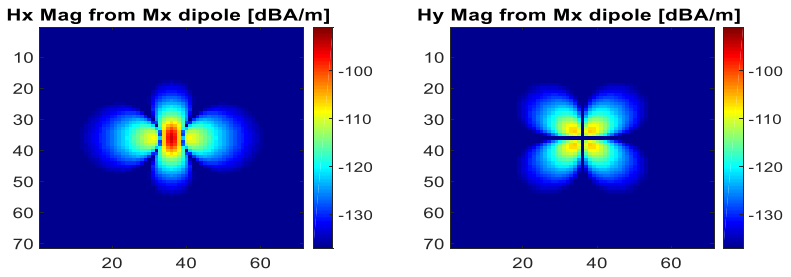

(b)

Figure 13. H_x and H_y patterns from the extracted dipole moments: (a) Magnitude of H_x and H_y from the most dominant dipole moment M_y. (b) Magnitude of H_x and H_y from the second most dominant dipole moment M_x

4. RF DESENSE APPLICATIONS

4.1. NUMERIC SIMULATION EXAMPLE

A simulation example of a RFI problem is discussed in this section. In Figure 14, the RFI between the unknown noise sources to the Wi-Fi patch antenna is studied. The patch is 37.2 mm× 28 mm. The unknown noise source is placed at the right side of the PCB. The unknown noise source generates the field pattern in Figure 11. The field is taken 3 mm above the noise source. Based on the work in [4] and [8], the forward problem and reverse problem are needed to predict coupling from noise source to antenna. In the forward problem, the real noise source is turned on and the victim antenna is turned off. In the reverse problem, the antenna is excited and the noise source is turned off. After the previous steps of machine learning based source reconstruction, the forward problem is solved and equivalent dipole moments for the noise source are extracted. In the reverse problem, transfer functions are obtained when the victim antenna radiates. Using the equivalent dipole moments and the transfer functions, the coupled voltage from the noise to the victim antenna can be analytically calculated.

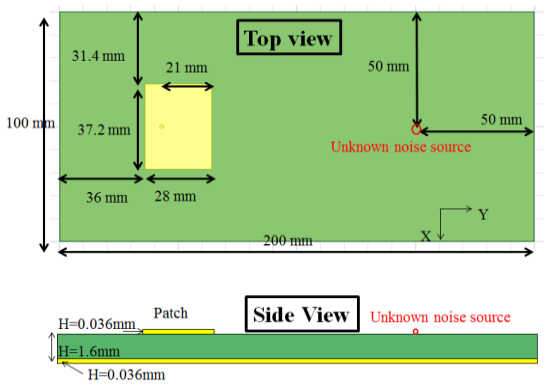

Figure 14. RFI from the unknown noise source to the patch antenna

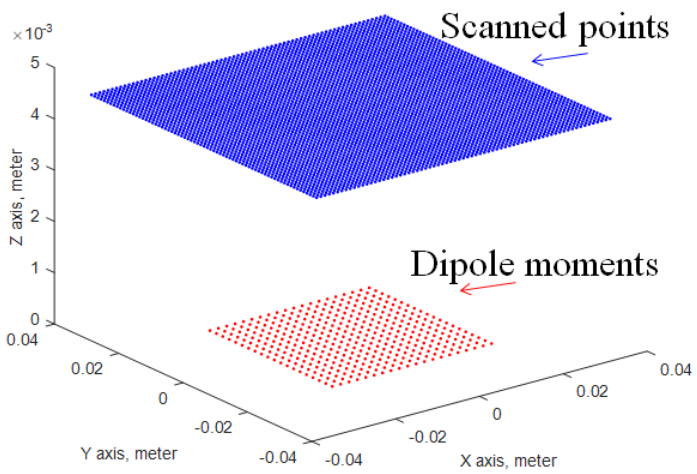

Figure 15. A total of 1200 dipole moments are used in conventional LSQ method

In order to show the correctness of the proposed method, the direct simulation is also performed for comparison. Similarly, the conventional LSQ method is further used to obtain the equivalent dipole moments for the noise source. An array of dipole moments is used. The dipole moments are uniformly placed at the points of 20 mm × 20 mm grid. There are three types of dipole moments (P_z, M_x, M_y) at each point. A total of 1200 dipole moments are used here, as shown in Figure 15. LSQ is utilized to solve the magnitude and phase of the 1200 dipole moments. Combining the 1200 dipole moments and the transfer functions from the reverse problem, the coupled voltage using this conventional LSQ method can also be obtained. The predicted RFI results from the machine learning based method and the conventional LSQ method are compared with direct simulation in Figure 16. In this ideal case, the proposed machine learning based method agrees with the direct simulation very well. The accuracy of the conventional LSQ method is worse than the machine learning based method.

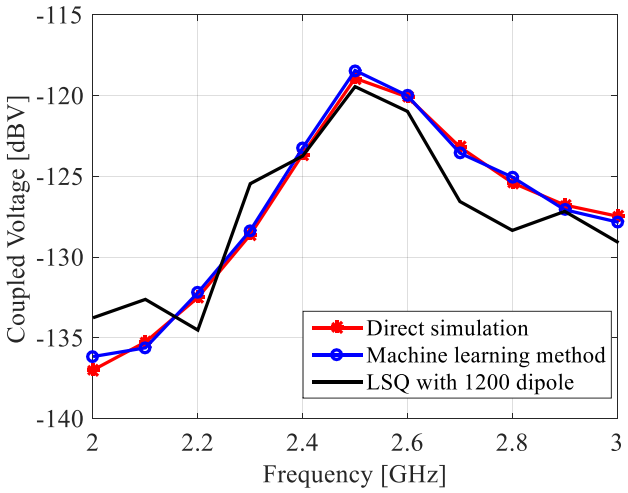

Figure 16. RFI comparisons from proposed machine learning method, conventional LSQ method and direct simulation

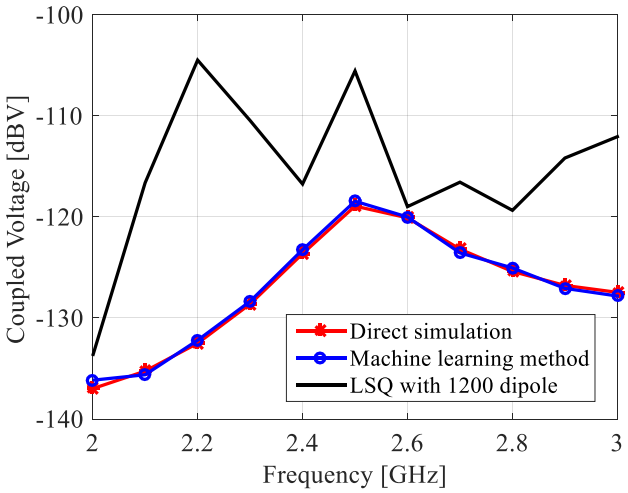

Figure 17. After adding noise to the field patterns, RFI comparisons from proposed machine learning method, conventional LSQ method and direct simulation

In order to mimic the noise effect in real world measurements, random noise is added to the field plots in Figure 11, the same procedures are repeated to compare the RFI from the machine learning based method, the conventional LSQ method and direct simulations. The result comparisons are shown in Figure 17. The proposed machine

learning method still works fine. The conventional LSQ method fails, as it is sensitive to noise especially when the number of unknowns is large.

4.2. MEASUREMENT VALIDATION USING A TEST BOARD

In this section, the measurement validation of the proposed method is performed using a simple test board. The RFI from a test IC to the above path antenna is studied. The test IC is a clock butter IC. The length and width of the IC is about 5 mm × 5 mm. Similarly as discussed in previous section, the forward problem and reverse problem are needed to predict coupling from noise source to the victim antenna. The measurement setup for the forward problem and the reverse problem is shown in Figure 18. The measured H_x and H_y magnitude are shown in Figure 19.

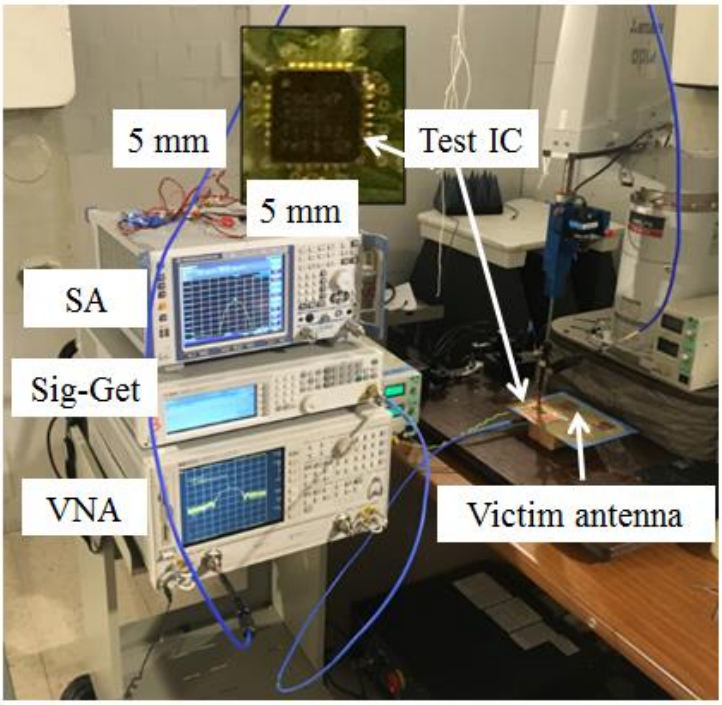

Figure 18. RFI from the noise IC to the patch antenna

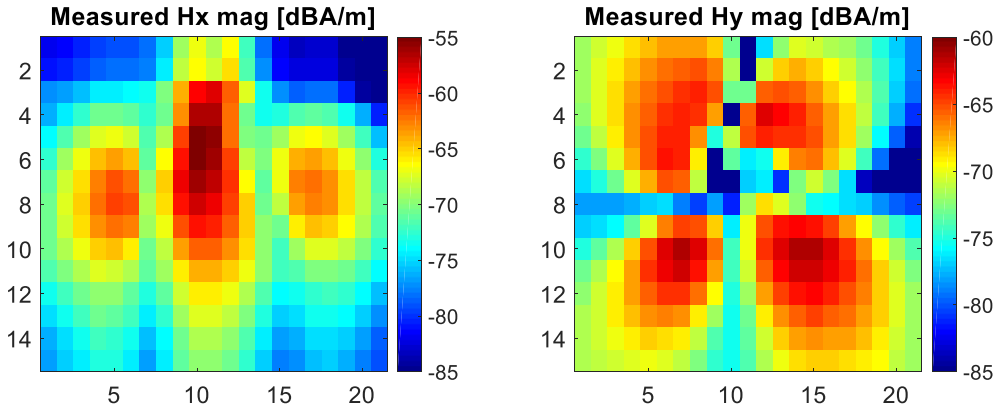

Figure 19. Measured H_x and H_y magnitude above the noise IC

According the proposed machine learning algorithm, the dominant dipole moment is identified as a M_x dipole moment. The contribution of the other types of dipole moments is negligible. It's clearly observed that the proposed machine learning based method can utilize the field patterns to find the correct location and minimal number of the dipole moments. In comparison, conventional LSQ method just simply uses a large array of dipole moments regardless of the field patterns [9]. The array of dipole moments is usually placed to cover the hot spot region. There is a high possibility that the location and number of the dipole moment array are incorrectly chosen. Nevertheless, a total number of 1200 dipole moments are used to reconstruct the noise IC in the conventional LSQ method. The predicted RFI results from the machine learning based method and the conventional LSQ method are compared with direct simulation in Figure 20. In this measurement example, the results from the proposed machine learning based method agree with the direct simulation very well, with the error less than 3 dB. The conventional LSQ method is much worse than the machine learning based method.

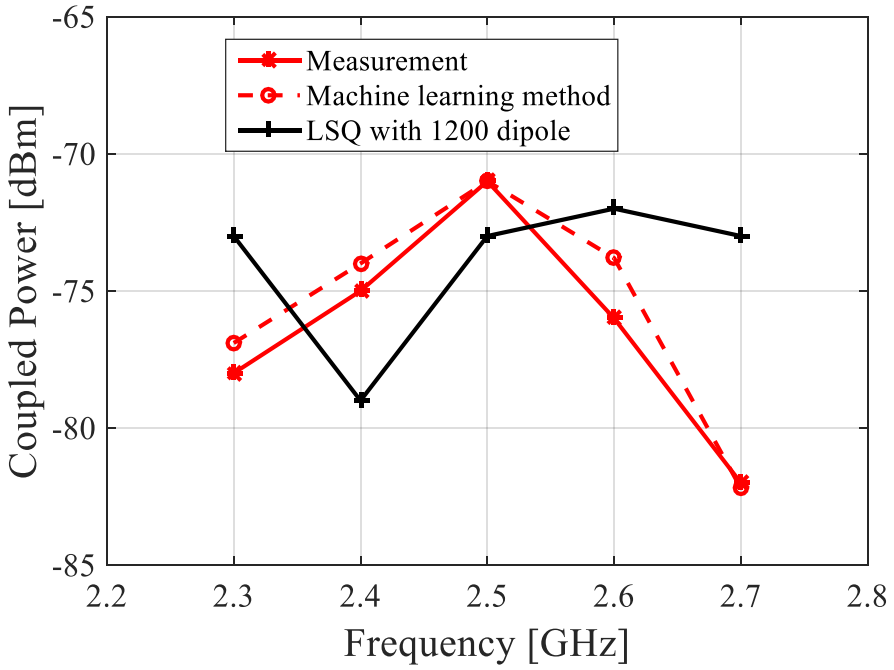

Figure 20. RFI comparison of the proposed machine learning method, conventional LSQ method and real measurement

The results also show that assigning more dipole moments for a noise source reconstruction is not necessarily a good choice. Noise effect and the overfitting issue are the main reasons why a large array of dipole moments can provide incorrect results. On contrast, in the machine learning based method, the noise effect is not that significant. Firstly, when training the SVM, different noise levels are added to the field patterns, as shown previously in Figure 4. The algorithm itself is well suitable to handle noise. Secondly, it's worthwhile to mention that the machine learning algorithm used in this work is SVM. Although SVM is powerful and simple to use, it's believed that recent deep learning algorithms [10], such as convolutional neural network [11] can provide an even better accuracy. The side effect of measurement noise can be well handled here.

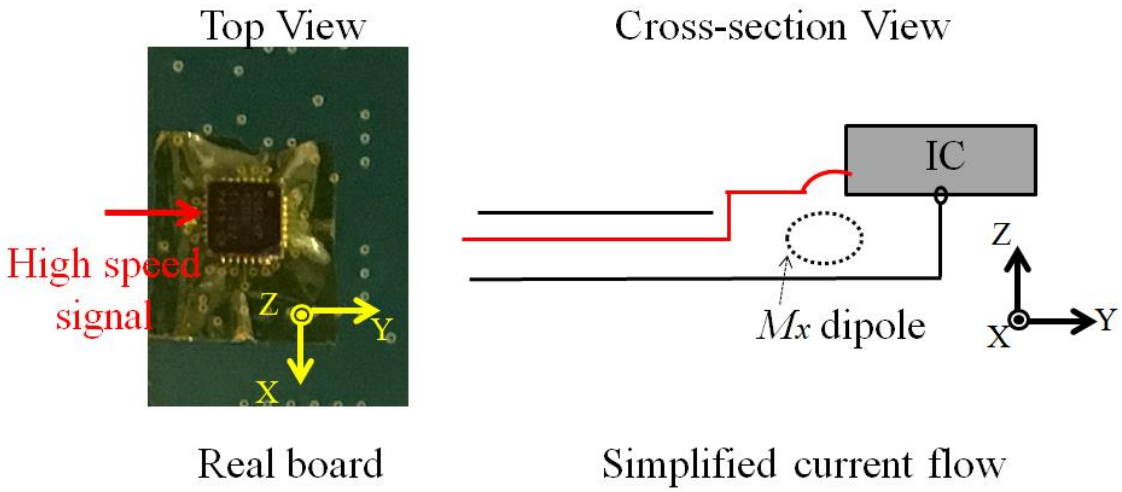

Figure 21. Physics of the M_x dipole moment

Another advantage of this machine learning based method is that the dominant dipole moments are provided. In this test IC, the dominant dipole moment is a single magnetic dipole moment M_x. The physics of how a M_x dipole moment is formed in this test IC is analyzed in Figure 21. From the left side, the high speed signal is routed inside the stripline structure. Because of the shielding effect of the solid ground, the radiation from the stripline part is negligible. The signal trace jumps from the inner part of the board to the top side in order to connect to the IC pin. The return current for the high speed signal is through the central ground pad. In this way, a current loop is formed in the *yz* plane. By definition, a current loop in the *yz* plane is a M_x dipole moment. Knowledge of the dominant dipole moment can help engineers to propose effective methods to solve RF desense issues. For instance, in this test board, reducing the magnitude of the M_x dipole moment can lead to a decrease of the coupling to the victim antenna. Reducing the current on the loop or reducing the loop size can both help achieve a smaller coupled noise on the victim antenna.

4.3. APPLICATION ON A REAL CELLPHONE PRODUCT

The proposed machine learning method is further applied on a real cellphone product in this section. After the near field scanning above the LCD, the magnitude of H_x and H_y are obtained, as shown in Figure 22. Using the proposed machine learning method, the dominant dipole moment is recognized as an M_y dipole. Other types of dipole moments are negligible. The workflow of extracting dipole moment is shown in Figure 23.

Knowing the source type provides a lot of insights. Firstly, the magnitude and phase of the equivalent dipole moment M_y can be obtained. Using the proposed method, the magnitude and phase of the H field for the measurement and dipole moment match well, as shown in Figure 24. The extracted dipole moment can be implemented in the full wave simulation software to perform RFI estimations.

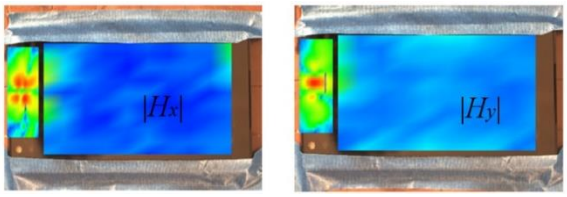

Figure 22. Magnitude of H_x and H_y field patterns above LCD of a cellphone

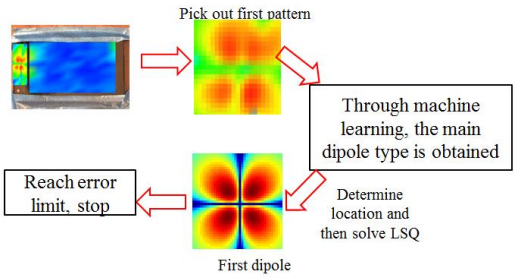

Figure 23. Workflow of the dipole moment extraction

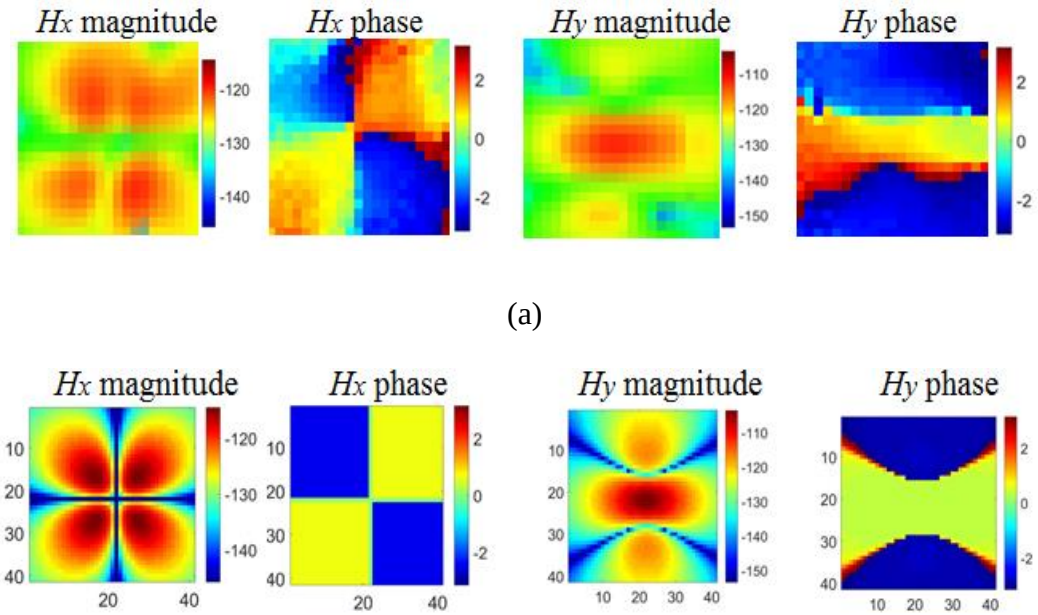

Figure 24.Magnitude and phase of H field from: (a) measurement of a real cellphone; (b) dipole moment M_y

Secondly, knowing the source type can help engineers to find the best placement of IC to minimize RFI. For example, Figure 25(a) gives the antenna model for this cellphone. Figure 25(b) shows the magnitude of H_y when the antenna radiates. In this problem, the noise source is identified as a M_y dipole moment. According to [8], the transfer function from each unit M_y dipole moment to the victim antenna is proportional to H_y when the victim antenna radiates in the reverse problem. So out of the locations 1 ,2 and 3, location 1 has the smallest transfer function and location 3 has the largest transfer function. In terms of RFI, location 1 is the best place to locate the noise source because the coupling between the M_y dipole moment to the victim antenna is the smallest at that location.

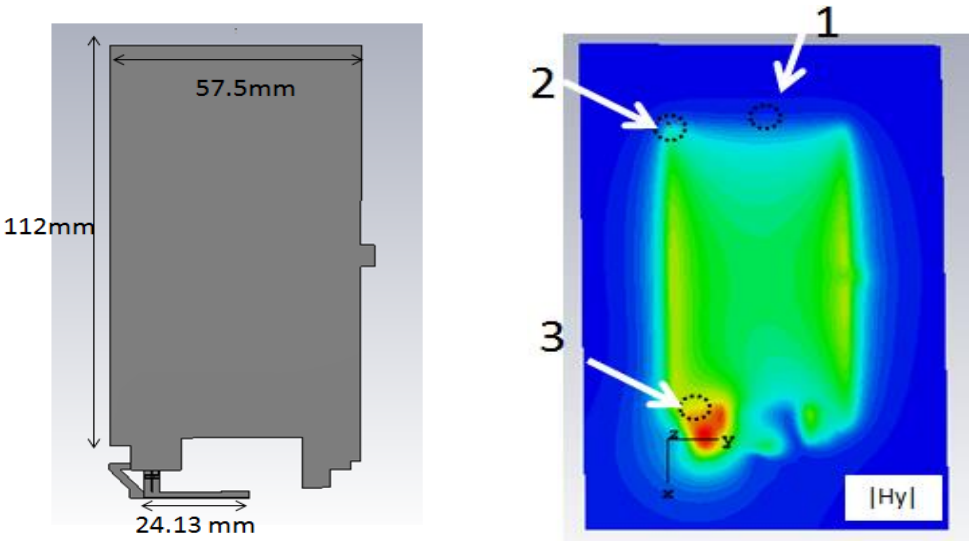

(a) (b)

Figure 25. (a)Antenna model, (b) Magnitude of H_y when the antenna radiates

5. CONCLUSION

In this paper, a machine learning based source reconstruction method is developed to extract the equivalent dipole moments for the noise source. The equivalent dipole moment method mainly has two advantages compared to Huygens' box method, as used in [12]-[14]. Firstly, Equivalent dipole moment method often requires the scanning measurement on one plane above the noise source to perform source reconstruction. In contrast, Huygens' box method needs 6-surface scanning, which introduces additional measurement time and difficulty because of the scanning on the side surfaces. Secondly, the Huygens' box can only deal with the electromagnetic fields on top of the Huygens' box and out of the box. Very few physical insights of the noise source inside the box can be obtained using Huygens' box method. However, an accurate dipole moment reconstruction can help find physical insights for the noise source, as shown in Figure 21

and [15]-[18]. In addition, previous dipole moment reconstruction methods, such as conventional LSQ and optimization method are affected by parameter selections, such as number and locations of dipole moments and choices of initial values. The machine learning based method in this paper can extract the equivalent dipole moments more accurately and reliably. Based on the near field patterns, the proposed method can determine the minimal number of dipole moments and their corresponding locations. Further the magnitude and phase for each dipole moment can be extracted. The proposed method can extract the most dominant dipole moments for the unknown noise source one by one. The proposed method is applied to a few theoretical examples first. Measurement validations using a test board and a practical cellphone are also given. Compared to the conventional LSQ method, the proposed machine learning based method is believed to have a better accuracy. Also, it's more reliable in handling noise in practical applications.

REFERENCES

[1] G. Y. Cho, J. Jin, H.-B. Park, H. H. Park, C. Hwang, "Assessment of Integrated Circuits Emissions with an Equivalent Dipole Moment Method", in IEEE Trans. Electromagn. Compat., vol. 59, no. 2, pp. 633-638, Dec 2016.

[2] J. Pan et al., "Radio-Frequency Interference Estimation Using Equivalent Dipole-Moment Models and Decomposition Method Based on Reciprocity," in IEEE Trans. Electromagn. Compat., vol. 58, no. 1, pp. 75-84, Feb. 2016.

[3] P. Fernndez Lpez, C. Arcambal, D. Baudry, S. Verdeyme and B. Mazari, "Simple electromagnetic modeling procedure: From near-field measurements to commercial electromagnetic simulation tool", in IEEE Trans. Instrum. Meas., vol. 59, no. 12, pp. 3111-3121, Dec. 2010.

[4] Z. Yu, J. A. Mix, S. Sajuyigbe, K. P. Slattery and J. Fan, "An Improved Dipole-Moment Model Based on Near-Field Scanning for Characterizing Near-Field Coupling and Far-Field Radiation From an IC," in IEEE Trans. Electromagn. Compat., vol. 55, no. 1, pp. 97-108, Feb. 2013.

[5] W. J. Zhao et al., "An Effective and Efficient Approach for Radiated Emission Prediction Based on Amplitude-Only Near-Field Measurements," in IEEE Trans. Electromagn. Compat., vol. 54, no. 5, pp. 1186-1189, Oct. 2012.

[6] J. Zhang and J. Fan, "Source Reconstruction for IC Radiated Emissions Based on Magnitude-Only Near-Field Scanning," in IEEE Trans. Electromagn. Compat., vol. 59, no. 2, pp. 557-566, April 2017.

[7] N. Dalal and B. Triggs, "Histograms of Oriented Gradients for Human Detection", in Proc. IEEE Conf. Computer Vision and Pattern Recognition, vol. 1, pp. 886-893, 2005.

[8] S. Lee et al., “Analytical intra-system EMI model using dipole moments and reciprocity,” submitted to Proc. IEEE Asia-Pac. Electromagn. Compat. Symp.,2018.

[9] L. Li, J. Pan, C. Hwang and J. Fan, "Radiation Noise Source Modeling and Application in Near-Field Coupling Estimation," in IEEE Trans. Electromagn. Compat., vol. 58, no. 4, pp. 1314-1321, Aug. 2016.

[10] Y. Bengio, I. J. Goodfellow, and A. Courville. Deep Learning. MIT Press, 2015.

[11] A. Krizhevsky, I. Sutskever, and G. Hinton, "ImageNet classification with deep convolutional neural networks," in Advances in Neural Information Processing Systems , pp. 1106–1114, 2012.

[12] L. Li, et al. “Near-Field Coupling Estimation by Source Reconstruction and Huygens’s Equivalence Principle.” Proc. IEEE Electromagn. Compat. Symp.,2015, pp. 324–329.

[13] L. Li, et al. “Radio-frequency interference estimation by reciprocity theorem with noise source characterized by Huygens's equivalent model” Proc. IEEE Electromagn. Compat. Symp.,2016, pp. 358–363.

[14] M. Sørensen, O. Franek and G. F. Pedersen, "Recent developments in using measured sources in computational EMC," 2015 9th European Conference on Antennas and Propagation (EuCAP), Lisbon, pp. 1-5, 2015.

[15] Q. Huang, F. Zhang, T. Enomoto, J. Maeshima, K. Araki and C. Hwang, "Physics-based dipole moment source reconstruction for RFI on a practical cellphone", in IEEE Trans. Electromagn. Compat., vol. 59, no. 6, pp. 1693-1700, Dec. 2017.

[16] Q. Huang et al., “Desense Prediction and Mitigation from DDR Noise Source,” in Proc. of IEEE Symp. Electromagn.Compat., 2018, pp. 139-144.

[17] Q. Huang et al., " MoM-Based Ground Current Reconstruction in RFI Application," IEEE Trans. Electromagn. Compat., vol. 60, no. 4, pp. 1121-1128, Aug. 2018.

[18] Q. Huang, Y. Chen, C. Hwang and J. Fan. “Machine Learning Based Source Reconstruction for RF Desensitization Analysis.” DesignCon 2018.

SECTION

2. CONCLUSIONS

With rapid innovations in Internet of Things (IoT) and wireless technology, more and more consumer electronic devices around the world are now connected to the internet. In a small form factor electronic device, there are plenty of potential RFI issues. Predicting and mitigating RFI issues are important for design engineers. The first paper focuses on deriving an analytical method to predict RFI. The second paper uses the derived equations in the first paper and proposes methods to mitigate RFI. In the third paper, a novel machine learning method is introduced to build equivalent dipole moments to replace noise sources.

In the first paper, a transfer function based calculation method is proposed to estimate RFI problems. The closed-form equations are analytically derived from Maxwell's equations and the reciprocity theorem. The RFI problem is decomposed into two parts: the noise source dipole moments and the coupling transfer function to the antenna. The transfer functions can be easily obtained from either simulation or measurement. Simple S_{21} measurements can help obtain transfer functions. The proposed method is validated through numeric simulations and real cellphone experiments. Engineers can utilize this method to identify root causes and propose mitigation solutions for RFI issues.

In the second paper, RFI reduction for a real consumer electronic device is studied. Considering the layout limitation of the product, the proposed RFI mitigation

involves rotating the CPU and DDR chip by a certain angle without compromising signal integrity. In addition to retaining signal integrity, the proposed method doesn't require shield can to meet RFI specification for achieving the desired Wi-Fi performance. New boards with the suggested changes were manufactured, and measured results showed a good RFI reduction (up to 8 dB) compared to the original board. The measured RFI reduction has a good agreement with theoretical RFI reduction. The proposed method enables a new dimension to RFI mitigation with cost-saving opportunities.

In the third paper, a machine learning based source reconstruction method is developed to extract the equivalent dipole moments for the noise source. The equivalent dipole moment method mainly has two advantages compared to Huygens' box method. Firstly, Equivalent dipole moment method often requires the scanning measurement on one plane above the noise source to perform source reconstruction. In contrast, Huygens' box method needs 6-surface scanning, which introduces additional measurement time and difficulty because of the scanning on the side surfaces. Secondly, the Huygens' box can only deal with the electromagnetic fields on top of the Huygens' box and out of the box. Very few physical insights of the noise source inside the box can be obtained using Huygens' box method. However, an accurate dipole moment reconstruction can help find physical insights for the noise source. In addition, previous dipole moment reconstruction methods, such as conventional LSQ and optimization method are affected by parameter selections, such as number and locations of dipole moments and choices of initial values. The machine learning based method in this paper can extract the equivalent dipole moments more accurately and reliably. Based on the near field patterns, the proposed method can determine the minimal number of dipole moments and their corresponding

locations. Further the magnitude and phase for each dipole moment can be extracted. The proposed method can extract the most dominant dipole moments for the unknown noise source one by one. The proposed method is applied to a few theoretical examples first. Measurement validations using a test board and a practical cellphone are also given. Compared to the conventional LSQ method, the proposed machine learning based method is believed to have a better accuracy. Also, it's more reliable in handling noise in practical applications.

BIBLIOGRAPHY

[1] Q. Huang, F. Zhang, T. Enomoto, J. Maeshima, K. Araki and C. Hwang, "Physics-based dipole moment source reconstruction for RFI on a practical cellphone", IEEE Trans. Electromagn. Compat., vol. 59, no. 6, pp. 1693-1700, Dec. 2017.

[2] Q. Huang, L Li, X Yan, B Bae, H Park, C Hwang, J Fanl., " MoM-Based Ground Current Reconstruction in RFI Application," IEEE Trans. Electromagn. Compat., vol. 60, no. 4, pp. 1121-1128, Aug. 2018.

[3] Q. Huang and J. Fan, “Machine Learning Based Source Reconstruction for RF Desense", IEEE Trans. Electromagn. Compat., vol. 60, no. 6, pp. 1640-1647, Dec. 2018.

[4] Q. Huang, T. Enomoto, J. Maeshima, K. Araki, J. Fan and C. Hwang, “Efficient RFI estimation and mitigation using dipole-moment based reciprocity" accepted to IEEE Trans. Electromagn. Compat.

[5] G. Maghlakelidze ,X. Yan ,L. Guan, S. Marathe , Q. Huang, B. Bae , C. Hwang ,V.Khilkevich , J. Fan , D. Pommerenke.,“ SNR Analysis and Optimization in Near-Field Scanning and EMI Applications", IEEE Trans. Electromagn. Compat., vol. 60, no. 4, pp. 1087-1094, Aug. 2018.

[6] S. Yang, Q. Huang, G. Li, R. Zoughi and D. Pommerenke, "Differential E-Field Coupling to Shielded H-Field Probe in Near-Field Measurements and a Suppression Approach," in IEEE Trans. Instrum. Meas., vol. 67, no. 12, pp. 2872-2880, Dec. 2018.

[7] Q. Huang, T. Enomoto, S. Seto, K. Araki, J. Fan and C. Hwang “Accurate and Fast RFI Prediction Based on Dipole Moment Sources and Reciprocity, DesignCon, 2018. (Best paper).

[8] Q. Huang, Y. Chen, C. Hwang and J. Fan“Machine Learning Based Source Reconstruction for RF Desensitization Analysis” DesignCon, 2018.

[9] Q. Huang, L. Zhang, Y. Zhong, J. Rajagopalan, D. Pai, C. Chen, A. Gaikwad, C. Hwang and J. Fan, “A Fast and Simple RFI Mitigation Method without Compromising Signal Integrity” DesignCon, 2019. (Best paper).

[10] Q. Huang, J. Li, J. Zhou, W. Wu, Y. Qi and J. Fan, "De-embedding method to accurately measure high-frequency impedance of an O-shape spring contact," in Proc. of IEEE Int. Symp. Electromagn.Compat., 2014, pp. 600-603.

[11] Q. Huang, L. Li, X. Yan, B. Bae, H. Park, C. Hwang and J. Fan, "MoM based current reconstruction using near-field scanning," in Proc. of IEEE Int. Symp. Electromagn.Compat., 2017, pp. 549-554.

[12] Q. Huang et al., “Desense Prediction and Mitigation from DDR Noise Source,” in Proc. of IEEE Symp. Electromagn.Compat., 2018, pp. 139-144.

[13] Q. Huang, Y. Liu, L. Li, Y. Wang, C.Wu and J. Fan, " Radio Frequency Interference Estimation Using Transfer Function Based Dipole Moment Model," in Proc. of IEEE Int. Symp. Electromagn.Compat., 2018. (Best paper)

[14] Q. Huang, Y. Zhong, Z. Sun,T. Enomoto, S. Seto, K. Araki ,J.Fan and C. Hwang " Reciprocity Theorem Based RFI Estimation for Heatsink Emission," accepted to Proc. of IEEE Int. Symp. Electromagn.Compat., 2019.

[15] Q.Huang, D. Pai, K. Rao, A. Mohan, J. Vutukury. C. Mieh, J. Fan and J. Rajagopalan, “Accurate prediction and mitigation of EMI from high-speed noise sources using full wave solver” accepted to Proc. of IEEE Int. Symp. Electromagn.Compat., 2019.

[16] C. Hwang and Q. Huang, "IC placement optimization for RF interference based on dipole moment sources and reciprocity," IEEE Asia-Pacific Electromagn. Compat. Symp., 2017, pp331-333.

[17] Y. Zhong, Q. Huang, T. Enomoto, S. Seto, K. Araki and C. Hwang " Measurement Based Characterization of Buzz Noise in Wireless Devices," accepted to Proc. of IEEE Int. Symp. Electromagn.Compat., 2018.

[18] S.Lee, Y. Zhong, Q. Huang, T. Enomoto, S. Seto, K. Araki, J. Fan and C. Hwang " Analytical Intra-System EMI Model using Dipole Moments and Reciprocity," accepted to Proc. of IEEE Int. Symp. Electromagn.Compat., 2018.

[19] C.Wu, Z. Sun, Q. Huang, Y. Wang, J. Zhou and J. Fan, “A Method to Extract Physical Dipoles for Radiating Source Characterization and Near Field Coupling Estimation” accepted to Proc. of IEEE Int. Symp. Electromagn.Compat., 2019.

[20] L. Zhang, Q. Huang, X.Su, D. Pai, J. Rajagopalan, A. Gaikwad, C. Hwang and J. Fan, “Accurate RFI Prediction of 3D Non-Planar Connector with Half Magnetic Dipole Pattern” accepted to APEMC, 2019.

VITA

Qiaolei Huang was born in Hanchuan, Hubei, China. He received his B.S. degree in Electronics and Information Engineering from Huazhong University of Science and Technology, Wuhan, China, in 2013. He joined the EMC Laboratory in the Missouri University of Science and Technology, Rolla, in 2013 and received the M.S. degree of Electrical Engineering in December 2016. He received his Ph.D. degree in Electrical Engineering in July 2019 from Missouri University of Science and Technology.

He received the best papers from DesignCon2018, DesignCon2019 and 2018 IEEE EMC symposium. His research interests included signal integrity, radio-frequency interference, near field scanning technology.